

Band gaps and spin-orbit splitting of ordered and disordered $\text{Al}_x\text{Ga}_{1-x}\text{As}$ and $\text{GaAs}_x\text{Sb}_{1-x}$ alloys

Su-Huai Wei and Alex Zunger

Solar Energy Research Institute, Golden, Colorado 80401

(Received 1 August 1988)

Spontaneous long-range ordering of the otherwise disordered isovalent semiconductor alloys $A_xB_{1-x}C$ has been recently observed in numerous III-V alloy systems exhibiting the CuAu-I, CuPt, and chalcopyrite structures. We present a theory for the ordering-induced changes in the Brillouin-zone-center electronic properties, with application to the $\text{Al}_x\text{Ga}_{1-x}\text{As}$ and $\text{GaAs}_x\text{Sb}_{1-x}$ alloys. The dominant effect for these systems is shown to be level repulsion between *different-symmetry* states of the binary constituents which fold into *equal-symmetry* states in the ordered ternary structures. Strong variations in the band gaps, spin-orbit splittings, and charge densities among the three basic ordered structures reflect the different magnitudes of the symmetry-enforced coupling between the folded states. An extension of the model to the disordered alloys yields good agreement with the observed optical bowing parameters for the fundamental gaps; however, the *positive* (downward concave) bowing of the spin-orbit splitting observed in some common-cation semiconductor alloy remains an unexplained puzzle.

I. INTRODUCTION

Isovalent ternary semiconductors $A_xB_{1-x}C$ formed by mixing the zinc-blende constituents AC and BC , constitute a group of technologically important materials as their structural, transport, and optical properties can be continuously tuned by varying the composition x , hence broadening the range of material properties available for specific applications.¹⁻⁶ Considerable efforts⁷⁻²⁷ have been devoted to understand the underlying physical mechanisms controlling the thermodynamic stability and electronic structure of both ordered and disordered isovalent ternary alloys. The traditional viewpoint⁷⁻⁹ on the thermodynamic stability of isovalent ternary alloys has been that the interaction between the AC and BC constituents is repulsive (since the alloy has positive formation enthalpy ΔH); hence the alloy will disproportionate at low temperatures into $AC+BC$; only at high temperatures (where the $-TS$ entropy term is dominant) can the disordered ("pseudobinary") phase be stably formed, exhibiting a typical zinc-blende diffraction pattern. This picture has been consistent with the then available experimental data^{7,8} and with simple model calculations.⁷⁻¹¹ Recently, however, Srivastava *et al.*¹³ and Mbaye *et al.*¹⁴ have predicted that at low-temperature isovalent semiconductor alloys with a large lattice-constant mismatch can form metastable *ordered* compounds (shown in Fig. 1) even though these ordered compounds have positive ΔH . These compounds are stabler than the disordered alloy with same composition but are unstable with respect to phase separation (which may, however, be kinetically very slow). In some special cases, even thermodynamically stable ordered compounds can be formed through strong chemical interaction [e.g., Si-C (Ref. 15) and $\text{Cd}_3\text{P}_2\text{-Zn}_3\text{P}_2$ (Ref. 16)], magnetic ordering (e.g.,¹⁷ ferromagnetic CdMnTe_2), or epitaxial growth¹⁸⁻²⁰ (e.g., Ga_2AsSb and GaInP_2). The reason for

this^{12-15,17-20} is that specific coherent ordered arrangements of A and B on a lattice can better minimize the strain energy than do disordered arrangements of the same composition. Recently, ordered $A_nB_{4-n}C_4$ compounds ($1 \leq n \leq 3$) with new diffraction patterns have been observed.²⁸⁻³⁶ These include InGaAs_2 ,^{28,29} Al-GaAs_2 ,³⁰ and Ga_2AsSb (Ref. 31) (formed in CuAu-I-like structure), Ga_2AsSb (Ref. 31) (formed in chalcopyrite structure) and Ga_2AsSb ,³² InGaP_2 ,³³ AlInAs_2 ,³⁴ and In-GaAs_2 (Ref. 35) (formed in CuPt-like structure). Compounds with famatinite and luzonite-like structures ($n=1$ or 3) have also been reported³⁶ to occur in $\text{Ga}_x\text{In}_{1-x}\text{As}$.

Phase-diagram calculations^{14,37} for bulk and epitaxial $A_xB_{1-x}C$ alloys have shown that ordering of the $A_nB_{4-n}C_4$ compounds can occur at the stoichiometric compositions $X_n = n/4 = \frac{1}{4}, \frac{1}{2}, \text{ and } \frac{3}{4}$, below some critical temperatures whose magnitudes, in real experiments, may depend on the surface properties (e.g., surface steps) and kinetic factors.^{33(a)} At intermediate compositions, one expects to find phase-coexistence regions (e.g., ordered plus disordered), whereas at higher temperatures a single-phase disordered structure may be obtained. Since it is now known that at the stoichiometric compositions X_n one can find either ordered or disordered structures (depending on the temperature and growth conditions), we conducted systematic investigation of the electronic structures of ordered isovalent ternary semiconductors, examining the extent to which the electronic structure of an ordered ternary compound differs from that of the disordered alloy of the same composition. Preliminary experimental results have indeed indicated noticeable changes in band gaps for $\text{Al}_{0.5}\text{Ga}_{0.5}\text{As}$,^{38,39} $\text{Ga}_{0.5}\text{In}_{0.5}\text{P}$,³³ and $\text{Ga}_{0.5}\text{In}_{0.5}\text{As}$,²⁸ depending on whether the growth conditions favored ordered or disordered alloys. While currently available ordered alloys exhibit imperfect ordering (i.e., ordered and antiphase domains), our calculation assumes perfect ordering, and, hence, ordering-

induced effects will be more pronounced.

This study is aimed at (i) developing an understanding of the basic differences between the electronic structure of ordered and disordered alloys, and (ii) aiding in the identification of ordered ternary compounds, through their electronic fingerprints.

The two systems we have chosen to study are the ordered common-anion $\text{Al}_n\text{Ga}_{4-n}\text{As}$ system, exhibiting near lattice match, and the lattice-mismatched common-cation $\text{Ga}_4\text{As}_n\text{Sb}_{4-n}$ system. Both systems have been observed³⁰⁻³² to form spontaneously ordered phases when grown on lattice-matched substrates.

Using self-consistent first-principles band-structure calculations we find that (i) the fundamental band gaps of the ordered ternary compounds are usually smaller than the linear average of the band gaps of the binary constituents due to symmetry-enforced level repulsion; (ii) the bowing parameter of the spin-orbit splitting Δ_0 is negative for common-cation ordered ternary compounds due to repulsion-induced localization; (iii) The magnitude of the level repulsion is strongly structure dependent (structural deformations leading to unequal bond lengths $R_{A-C} \neq R_{B-C}$ enhance this level repulsion); (iv) for $\text{Al}_x\text{Ga}_{1-x}\text{As}$ we find that the concentration variation of the band gaps cannot be fitted to a quadratic equation. The optical bowing parameters calculated using the supercell approach are in good agreement with experimental observation.

II. EVOLUTION OF THE ELECTRONIC STRUCTURE OF ORDERED TERNARY COMPOUNDS FROM THAT OF THE BINARY CONSTITUENTS: QUALITATIVE PHYSICS

In this section we describe the way in which the electronic structure of the ordered ternary semiconductors

can be described as a perturbation on the electronic structure of the binary constituents. While our actual calculation (Sec. V) treats the ordered ternary systems as new compounds in their own right without involving perturbation theory, the present section, using arguments of perturbation theory, will serve to establish the basic qualitative chemical trends. An analogous discussion of the evolution of the electronic structure of disordered alloys from that of ordered compounds is given in Sec. VI.

A. Choice of ordered ternary structures

The Landau-Lifshitz theory⁴⁰ of phase transitions provides simple rules for selecting a small number of ordered structures which can interconvert, under well-defined constraints, into disordered phases of the same composition. The conditions for selecting these ordered phases are^{40,41} (i) the space group of the ordered structure must be a subgroup of that of the disordered alloy, and (ii) the ordered structure must be associated with an ordering vector located at a special \mathbf{k} point of the parent space group. These ordered structures have the following properties:^{40,41} (i) the order-disorder phase transition can be of second order (but need not be). (ii) The ordered structures are stable with respect to antiphase boundaries. (iii) They can occur over a wide concentration range in the phase diagram. Figure 1 shows five of the small-unit-cell structures obtained in this way (along with the zincblende structure) with information about their structural symmetries. These sets can be organized into four groups according to the ordering vectors (in units of $2\pi/a$): (i) For the (0,0,0) ordering vector we have the zinc-blende lattice of the binary constituents AC and BC , (ii) for the (0,0,1) ordering vector we have at 50%-50% composition the layered tetragonal (CuAu-I -like structure, denoted

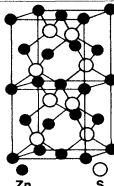
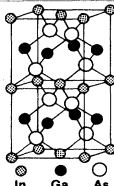
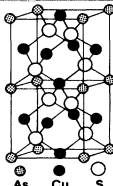
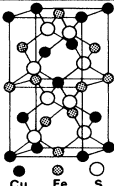
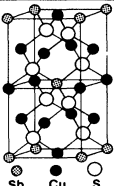
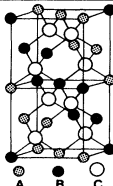
Ordering Vectors	(0,0,0)	(0,0,1)	(2,0,1)		(1,1,1)	
Name (ternary)	Zincblende (Sphalerite)	Layered Tetragonal	"Luzonite"	Chalcocopyrite	Famatinite	Layered Trigonal
Formula	n = 0.4;AC	n = 2;ABC ₂	n = 1.3; A ₃ BC ₄	n = 2;ABC ₂	n = 1.3; A ₃ BC ₄	n = 2;ABC ₂
						
Example (ternary)	ZnS type	InGaAs ₂ type	Cu ₃ AsS ₄ type	CuFeS ₂ type	Cu ₃ SbS ₄ type	CrCuS ₂ type (Na V S ₂)
Bravais Lattice	Face centered cubic	Simple tetragonal	Simple cubic	Body centered tetragonal	Body centered tetragonal	Rhombohedral
Space Group	$F\bar{4}3m$	$P\bar{4}m2$	$P\bar{4}3m$	$i\bar{4}2d$	$i\bar{4}2m$	$R\bar{3}m$
Int. Tables	T_d^2	D_{2d}^5	T_d^1	D_{2d}^{12}	D_{2d}^{11}	C_{3v}^5
Schoenflies	T_d	T_d	T_d	D_{2d}	D_{2d}	C_{3v}
Number	216	115	215	122	121	160
Strukturbericht	B3	H2 ₄	E1 ₁	H2 ₄	H2 ₄	
Pearson symbol	CF8	CP8	CP8	II16	II16	hR4
Atomic positions (ternary)	Zn: 4 a $\bar{4}3m$ S: 4 c $\bar{4}3m$	1A: 1 a $\bar{4}2m$ 1B: 1 c $\bar{4}2m$ 2C: 2 g mm	3 Cu: 3 c $\bar{4}2m$ 1 As: 1 a $\bar{4}3m$ 4 S: 4 e 3m	2 Cu: 4 a $\bar{4}$ 2 Fe: 4 b $\bar{4}$ 4 S: 8 d 2	1 Cu: 2 b $\bar{4}2m$ 2 Cu: 4 d $\bar{4}$ 1 Sb: 2 a $\bar{4}2m$ 4 S: 8 i m	1 A: 1 a 3m 1 B: 1 a 3m 1 C: 1 a 3m 1 C: 1 a 3m
Equivalent superlattice	None	(1,1) in [0 0 1] direction	None	(2,2) in [2 0 1] direction	(1,3) in [2 0 1] direction	(1,1) in [1 1 1] direction

FIG. 1. Crystal structures of small-unit-cell Landau-Lifshitz $A_nB_{4-n}C_4$ ordered fcc phases. See text (Sec. II A) for discussion.

here as "CA") and at 25%-75% or 75%-25% composition the luzonite-like structure (denoted here as "L"). (iii) For the $(1,0,\frac{1}{2})$ ordering vector [sometimes denoted $(2,0,1)$], we have at 50%-50% composition the chalcopyrite structure (denoted here as "CH"), whereas for 25%-75% or 75%-25% composition we have the famatinite structure (denoted here as "F"). Finally, (iv) for the $(\frac{1}{2},\frac{1}{2},\frac{1}{2})$ ordering vector [sometimes denoted $(1,1,1)$], we have at the 50%-50% composition the layered trigonal CuPt-like structure (denoted here as "CP").

Since the information on these structures is scattered in numerous literature sources, and since different notations are used in these sources, we give in Fig. 1 a comprehensive list of notations. For instance, to find the space group operations, use the *International Tables for Crystallography*⁴² under the space-group number given in Fig. 1. To find other compounds belonging to these structure types and the atomic-position coordinates, use *Pearson's Handbook of Crystallographic Data for Intermetallic Phases*⁴³ according to the "Pearson symbol" given in Fig. 1. Information regarding the structural chemistry of these phases can be found in Ref. 44, designated according to the Strukturbericht symbol given in Fig. 1. Statistical-mechanics descriptions of configurational ordering in these Landau-Lifshitz structures (e.g., Refs. 40, 41, and 45) are designated according to the "ordering vectors." Figure 1 also indicates (where applicable) the type of superlattice which is structurally equivalent to these compounds. Finally, the structural and thermodynamic properties given in metallurgical literature (e.g., Refs. 46 and 47) are denoted according to the chemical formula ("example" of Fig. 1), whereas information regarding the Brillouin zones (Ref. 48) are often designated according to the Schoenflies notation given in Fig. 1.

The unit-cell vectors and atomic-position coordinates for the CuAu-I, chalcopyrite, luzonite, and famatinite structures were given in Ref. 19, whereas those for the CuPt structure are depicted in Ref. 15. We have assumed all these systems to be cubic (i.e., no symmetry-allowed tetragonal or trigonal distortion of the AB sublattice), since optimization of the total energy for these systems^{37,49} shows such distortions to be less than 1%.

Among the four groups of structures seen in Fig. 1, the set of the $(0,0,1)$ ordering vectors has a special significance in the context of the disordered alloy: they are the structures with the smallest unit cell, each exhibiting a single type of local cluster (A_4 , A_3B , A_2B_2 , AB_3 , and B_4 in zinc-blende, luzonite, CuAu-I, luzonite, and zinc-blende structure, respectively). They are often used as building blocks (tetrahedra) to mimic the disordered alloys.

B. Folding relationships and their consequences

To illustrate the generic relationships between the electronic structure of ordered ternary compounds and their isovalent binary constituents AC and BC , consider first the three conduction states Γ_{1c} , L_{1c} , and X_{1c} of AC and BC (Fig. 2, where C is assumed to be here the common cation). As the zeroth-order model for the corresponding energy levels of the ternary phase (either ordered or

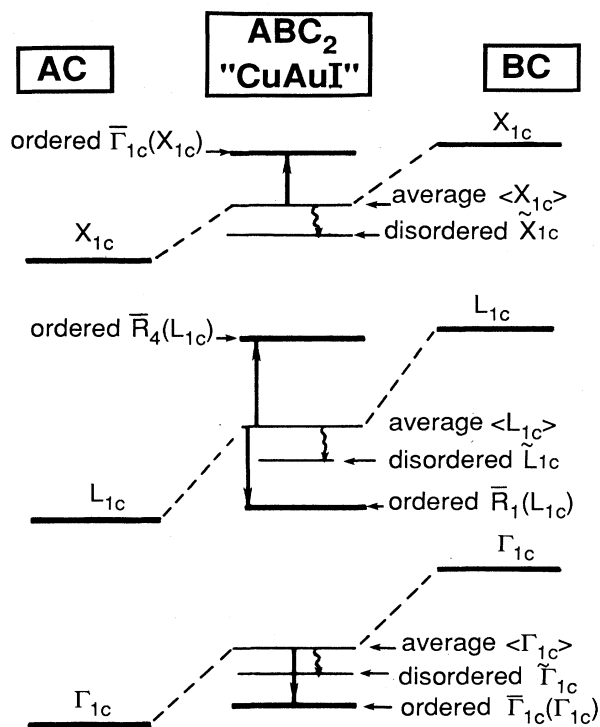


FIG. 2. Schematic plot showing the evolution of the electronic state $\bar{\Gamma}_{1c}$, \bar{R}_{1c} , and \bar{R}_{4c} of an ordered ABC_2 common-cation compound and the states $\bar{\Gamma}_{1c}$, \bar{X}_{1c} , and \bar{L}_{1c} of a disordered $A_{0.5}B_{0.5}C$ alloy from the states of the binary constituents AC and BC .

disordered), we take the linear, concentration-weighted average of the corresponding energies in the binaries. These averages are denoted in Fig. 2 as $\langle \Gamma_{1c} \rangle$, $\langle L_{1c} \rangle$, and $\langle X_{1c} \rangle$. Experimentally^{1-3,50,51} and theoretically,^{26-27,52-57} it is known that the energy levels of the disordered alloy usually lie below these average energies (we return to a theoretical discussion of the origin of this "optical bowing" effect in Sec. VI). The energies of the disordered phase are denoted in Fig. 2 as $\bar{\Gamma}_{1c}$, \bar{L}_{1c} , and \bar{X}_{1c} . It is instructive to classify the electronic states of ordered ternary compounds, according to the band (m) and wave-vector \mathbf{k} states $|m, \mathbf{k}\rangle$ of the binary constituents folded into the smaller ternary Brillouin zone. Tables I–III give these folding relationships for the structure of Fig. 1, i.e., for $(0,0,1)$ (Table I), $(1,0,\frac{1}{2})$ (Table II), and $(\frac{1}{2},\frac{1}{2},\frac{1}{2})$ (Table III) ordering vectors. Note that the representations of the folded states are generally different for common-anion and common-cation ternary structures.

The significant content of Tables I–III for the present discussion is that states of different symmetry in the binary constituents can fold into states of the same symmetry in the ternary system. In the particular example of common-cation CuAu-I-like ordering illustrated in the center column of Fig. 2, we show two $\bar{\Gamma}_1$ -folded states: $\bar{\Gamma}_{1c}$ (Γ_{1c}) and $\bar{\Gamma}_{1c}$ (X_{1c}). (The L_{1c} -type state folds into itself and generates the \bar{R}_4 and \bar{R}_1 representations which are discussed in Ref. 25.) One can image an "unper-

TABLE I. Mapping (folding relationships) of the zinc-blende (ZB) Γ and X states into ABC_2 CuAu-I-like states and A_3BC_4 luzonite-like states at the center of the Brillouin zone. The origin of the coordinate system in ZB is at the anion site.

ZB	ABC_2 , CuAu		A_3BC_4 , luzonite	
	Common anion	Common cation	Common anion	Common cation
Γ_1	$\bar{\Gamma}_1$	$\bar{\Gamma}_1$	$\bar{\Gamma}_1$	$\bar{\Gamma}_1$
Γ_{15}	$\bar{\Gamma}_5 + \bar{\Gamma}_4$	$\bar{\Gamma}_5 + \bar{\Gamma}_4$	$\bar{\Gamma}_{15}$	$\bar{\Gamma}_{15}$
X_1	$\bar{\Gamma}_4$	$\bar{\Gamma}_1$	$\bar{\Gamma}_{15}$	$\bar{\Gamma}_1 + \bar{\Gamma}_{12}$
X_3	$\bar{\Gamma}_1$	$\bar{\Gamma}_4$	$\bar{\Gamma}_1 + \bar{\Gamma}_{12}$	$\bar{\Gamma}_{15}$
X_5	$\bar{\Gamma}_5$	$\bar{\Gamma}_5$	$\bar{\Gamma}_{15} + \bar{\Gamma}_{25}$	$\bar{\Gamma}_{15} + \bar{\Gamma}_{25}$

turbed" crystal potential for the ternary structure such that the states $\bar{\Gamma}_{1c}$ (Γ_{1c}) and $\bar{\Gamma}_{1c}$ (X_{1c}) would be degenerate with the average energies $\langle \Gamma_{1c} \rangle$ and $\langle X_{1c} \rangle$, respectively. Despite the fact that a seemingly new direct state $\bar{\Gamma}_1$ (X_{1c}) is generated in the ternary structure, in the absence of a potential perturbation the no-phonon transition matrix element from valence-band Γ states is, of course, still precisely zero, just as is the case for transitions to the X_{1c} state from which it is folded.

In reality, however, there exists an ordering potential perturbation $\Delta V(\mathbf{r})$ distinguishing energy levels of the ternary system from the average energy levels of the binaries. This potential does not have zinc-blende symmetry, but belongs instead to the totally symmetric representation of the space group of the *ternary* structure. In general, $\Delta V(\mathbf{r})$ has a electronic piece, contributed by the electronegativity difference between the alloyed atoms A and B (as reflected, for example, by differences in their atomic-orbital energies, given in Table IV) and a structural piece, due to possible atomic displacements in the ternary phase relative to ideal zinc-blende positions. This ordering potential $\Delta V(\mathbf{r})$ can couple the zinc-blende states $|\gamma_i, m, \mathbf{k}\rangle$ and $|\gamma_j, m', \mathbf{k}'\rangle$ if they fold into states belonging to the same representation $\bar{\gamma}$. Using perturbation theory, the energy shift due to the coupling of the zinc-blende states $|\gamma_i, \mathbf{k}\rangle$ and $|\gamma_j, \mathbf{k}'\rangle$ folded into states of the same symmetry $\bar{\gamma}$ in the ternary phase (at wave vector \mathbf{K}) is

$$\delta E(\bar{\gamma}, \mathbf{K}) = \pm \frac{|\langle \gamma_i, m, \mathbf{k} | \Delta V(\mathbf{r}) | \gamma_j, m', \mathbf{k}' \rangle|^2}{\epsilon_m(\mathbf{k}) - \epsilon_{m'}(\mathbf{k}')} \quad (1)$$

This repulsion is indicated schematically for the $\{\bar{\Gamma}_{1c}$ (Γ_{1c}); $\bar{\Gamma}_{1c}$ (X_{1c}) $\}$ pair in Fig. 2 by the solid vertical arrows. The downward-repelled $\bar{\Gamma}_{1c}$ (Γ_{1c}) state could, under specific circumstances (see Sec. V), be lower in energy than the state $\bar{\Gamma}_{1c}$ of the disordered alloy. The new $\bar{\Gamma}_{1c}$ (X_{1c}) state becomes "pseudodirect" and can have a finite matrix element for Γ transitions from the valence bands.

This simple analysis points to a number of qualitative features which will be examined quantitatively in the next section.

(i) Significant level repulsion can be expected between those states of same symmetry for which the energy denominator of Eq. (1) is small. To assess these energies, we give the linear concentration-weighted average energies for GaSb-GaAs and AlAs-GaAs in Figs. 3 and 4, respectively. Comparison with Tables I–III shows that in GaSb-GaAs the energy denominator is smaller for the CuPt-folded states $\{\bar{\Gamma}_{1c}$ (Γ_{1c}); $\bar{\Gamma}_{1c}$ (L_{1c}) $\}$ than for the CuAu-I-folded states $\{\bar{\Gamma}_{1c}$ (Γ_{1c}); $\bar{\Gamma}_{1c}$ (X_{1c}) $\}$; therefore we will expect a larger level repulsion in the CuPt structure. For the chalcopyrite structure, Table II predicts but a small level repulsion between $\bar{\Gamma}(\Gamma)$ and $\bar{\Gamma}(W)$ since the energy denominator $\epsilon(\Gamma) - \epsilon(W)$ near the band edge is rather large in the binary constituents (see Table VII below). Similarly, since the $\langle \Gamma_{1c} \rangle - \langle X_{1c} \rangle$ energy separa-

TABLE II. Mapping (folding relationships) of the zinc-blende (ZB) Γ , X , and W states into ABC_2 chalcopyrite states and A_3BC_4 famatinite states at the center $\bar{\Gamma}$ of the Brillouin zone. The origin of the coordinate system for ZB is at the anion site.

ZB	Chalcopyrite ABC_2		Famatinite A_3BC_4	
	Common anion	Common cation	Common anion	Common cation
Γ_1	$\bar{\Gamma}_1$	$\bar{\Gamma}_1$	$\bar{\Gamma}_1$	$\bar{\Gamma}_1$
Γ_{15}	$\bar{\Gamma}_4 + \bar{\Gamma}_5$	$\bar{\Gamma}_4 + \bar{\Gamma}_5$	$\bar{\Gamma}_4 + \bar{\Gamma}_5$	$\bar{\Gamma}_4 + \bar{\Gamma}_5$
X_1	$\bar{\Gamma}_2$	$\bar{\Gamma}_3$	$\bar{\Gamma}_4$	$\bar{\Gamma}_1$
X_3	$\bar{\Gamma}_3$	$\bar{\Gamma}_2$	$\bar{\Gamma}_1$	$\bar{\Gamma}_4$
X_5	$\bar{\Gamma}_5$	$\bar{\Gamma}_5$	$\bar{\Gamma}_5$	$\bar{\Gamma}_5$
W_1	$\bar{\Gamma}_5$	$\bar{\Gamma}_1 + \bar{\Gamma}_3$	$\bar{\Gamma}_5$	$\bar{\Gamma}_1 + \bar{\Gamma}_3$
W_2	$\bar{\Gamma}_5$	$\bar{\Gamma}_2 + \bar{\Gamma}_4$	$\bar{\Gamma}_5$	$\bar{\Gamma}_2 + \bar{\Gamma}_4$
W_3	$\bar{\Gamma}_1 + \bar{\Gamma}_3$	$\bar{\Gamma}_5$	$\bar{\Gamma}_1 + \bar{\Gamma}_3$	$\bar{\Gamma}_5$
W_4	$\bar{\Gamma}_2 + \bar{\Gamma}_4$	$\bar{\Gamma}_5$	$\bar{\Gamma}_2 + \bar{\Gamma}_4$	$\bar{\Gamma}_5$

TABLE III. Mapping (folding relationships) of the zincblende (ZB) Γ and L states into ABC_2 CuPt-like states at the center of the Brillouin zone. Origin at the anion site.

ZB	Common anion	Common cation
Γ_1	$\bar{\Gamma}_1$	$\bar{\Gamma}_1$
Γ_{15}	$\bar{\Gamma}_1 + \bar{\Gamma}_3$	$\bar{\Gamma}_1 + \bar{\Gamma}_3$
L_1	$\bar{\Gamma}_1$	$\bar{\Gamma}_1$
L_3	$\bar{\Gamma}_3$	$\bar{\Gamma}_3$

tion decreases slightly in GaSb-GaAs as the As composition increases (Fig. 3), we expect a greater level-repulsion effect in the As-rich luzonite (Ga_4SbAs_3) than in the As-poor luzonite ($\text{Ga}_4\text{Sb}_3\text{As}$). In the AlAs-GaAs system, the isosymmetric states are $\{\bar{\Gamma}_{1c}(\Gamma_{1c}); \bar{\Gamma}_{1c}(X_{3c})\}$. The decrease in the $\langle \Gamma_{1c} \rangle - \langle X_{3c} \rangle$ separation as the Al content increases (Fig. 4) hence suggests a greater level repulsion for the Al-rich luzonite (GaAl_3As_4) than for the Ga-rich luzonite (Ga_3AlAs_4).

(ii) The numerator of Eq. (1) can sensitively control level repulsion between states with different angular-momentum character. For example, isovalent mixed-cation systems (e.g., GaAs-AlAs and GaP-InP) are expected to have a small matrix element between p -like states since isovalent cations have generally similar p -orbital energies (see Table IV). Since the upper valence band comprises primarily p orbitals, we expect in this case a weak valence-band level-repulsion effect. In contrast, since isovalent anions have rather different p -orbital energies (e.g., Table IV), mixed-anion systems (e.g., GaAs-GaSb) are expected to have a substantial matrix element between p -like states, and, hence, a substantial level-repulsion effect in the p -like valence band. Since both mixed-cation and mixed-anion systems have sub-

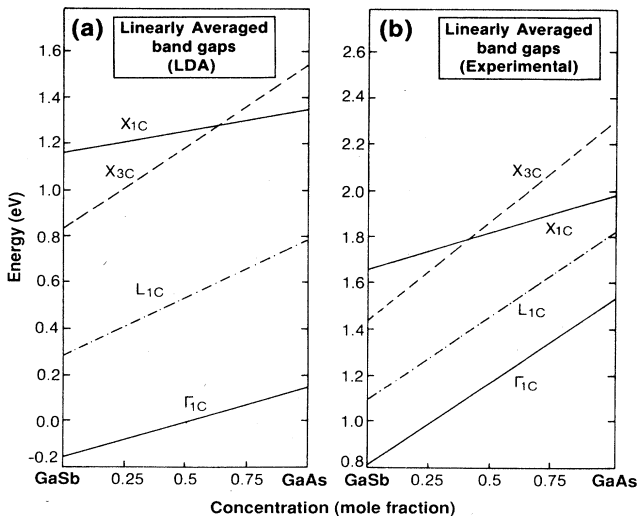


FIG. 3. Linear average of the conduction-band energies of GaSb-GaAs: (a) using the local-density approximation (LDA) and (b) experimental values of Ref. 82.

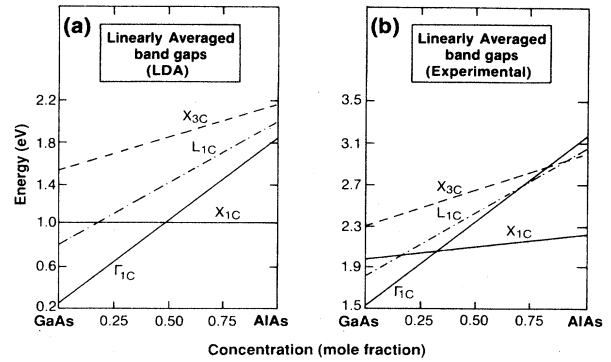


FIG. 4. Linear average of the conduction-band energies of GaAs-AlAs: (a) using the local-density approximation (LDA) and (b) experimental values of Ref. 82.

stantially different s -like orbital energies (Table IV), we expect a large coupling between s -like states, and, hence, significant level repulsion in s -like conduction bands.

(iii) Since the Γ_{1c} wave function is comprised of cation s + anion s orbitals, only folded states which have large s character in the mixed sublattice can be expected to significantly couple to it. For a mixed-cation system, this is the case for X_{3c} (cation s and anion p state) and L_{1c} (mostly s -like state); for mixed-anion systems, this is the case for X_{1c} (cation p + anion s state) and L_{1c} states.

(iv) The relative phase⁵⁸ of the states $|\gamma_i, m, \mathbf{k}\rangle$ and $|\gamma_j, m', \mathbf{k}'\rangle$ can determine the numerator of Eq. (1): the coupling matrix element $\langle \mathbf{k} | \Delta V(\mathbf{r}) | \mathbf{k}' \rangle$ is large only if the ordering potential $\Delta V(\mathbf{r})$ is in phase with the wave-vector difference $\mathbf{k} - \mathbf{k}'$. This is the case for the CuPt-like and CuAu-I-like structures where the ordering vectors $(2\pi/a)(0, 0, 1)$ and $(2\pi/a)(\frac{1}{2}, \frac{1}{2}, \frac{1}{2})$, respectively, are in exact registry with the wave-vector difference of the coupling $\Gamma - X$ and $\Gamma - L$ states, respectively. For the chalcopyrite structure, however, the ordering vector $(2\pi/a)(1, 0, \frac{1}{2})$ does not match the wave-vector difference $(2\pi/a)(0, 0, 1)$ of the coupling Γ and X_z states. One can see that the lowest Fourier component of $\Delta V(\mathbf{r})$ of the chalcopyrite structure $V_G = (2\pi/a)(0, 0, 1)$ which can couple the Γ and X_z states is identically zero since the planar-averaged potential of chalcopyrite structure has the period of $a/2$ (Fig. 1). In fact, one can prove that because of the *nonsymorphic* space group of chalcopyrite many of the Fourier components which couple the Γ and X states vanish because they have zero phase factors.

(v) Level repulsion between $|\mathbf{k}\rangle$ and $|\mathbf{k}'\rangle$ can localize

TABLE IV. Calculated s and p atomic LDA orbital energies (in eV) of Al, Ga, As, and Sb using the Hedin-Lundqvist correlation potential (Ref. 65).

	Al	Ga	As	Sb
ϵ_s	-7.91	-9.25	-14.77	-13.16
ϵ_p	-2.86	-2.82	-5.42	-5.08

the wave function on different sublattices in $A_n B_{4-n} C_4$. The degree of this localization is strongly correlated with the energy shift δE of Eq. (1). This repulsion-induced level localization is analogous to that described in tight-binding models⁵⁹ for zinc-blende compounds, where level repulsion causes the bonding states (shifting to lower energies) to localize on the anion sites, whereas the antibonding states (shifted to higher energies) localize on the cation site (since the anion has lower s - and p -orbital energies than the cation). This repulsion-induced localization will have important effects on the spin-orbit splitting which depends primarily on the degree of wave-function localization near a given atomic site.

(vi) Since in ternary tetrahedral semiconductors the Γ_{15} -like top of the valence band (p -like) is usually repelled upwards and the Γ_{1c} -like bottom of the conduction band (s -like) is repelled downwards, this model explains the experimentally observed positive (downward) bowing of the fundamental band gap of these ternary systems. However, the same mechanism also suggests that higher-energy states [e.g., Γ_{1c} (X_{1c}) in Fig. 2] could be shifted to yet higher energies^{60,61} when the relevant repelling state is lower in energy.

Having established the general physical principles governing the trends in the energy-level shifts between binary and ternary compounds, we turn to a quantitative discussion of the calculated results.

III. METHOD OF CALCULATION

We have used the self-consistent general-potential linear augmented-plane-wave (LAPW) method⁶² within the local-density-functional approximation⁶³ (LDA) to calculate the electronic structures of $Ga_4As_nSb_{4-n}$ (using the Ceperley-Alder exchange-correlation functional as parametrized by Perdew and Zunger⁶⁴) and $Al_nGa_{4-n}As_4$ (using the Hedin-Lundqvist⁶⁵ exchange-correlation functional). For GaAs we find that these two exchange-correlation functionals give the same eigenvalues to within 0.01 eV. Scalar-relativistic effects are included and spin-orbit splittings are calculated through a second variational procedure.⁶⁶ The shallow Ga $3d$ states are treated with spherical potentials and the small amount of Ga $3d$ density spilling outside the muffin-tin (MT) spheres is treated exactly, using an overlapping scheme, without further approximation.⁶² The core states as well as valence states are treated self-consistently. All the convergence parameters, including the muffin-tin radii, basis sets, and Brillouin-zone k -point samplings are kept the same for all structures to avoid random errors. The two special k points⁶⁷ used for the zinc-blende structure are

$$\mathbf{k}_1 = (2\pi/a)(\frac{1}{4}, \frac{1}{4}, \frac{1}{4}), \quad \omega_1 = \frac{1}{4} \quad (2a)$$

$$\mathbf{k}_2 = (2\pi/a)(\frac{1}{4}, \frac{3}{4}, \frac{1}{4}), \quad \omega_2 = \frac{3}{4} \quad (2b)$$

where a is the cubic lattice constant and ω is the weight of the corresponding k point. The equivalent k points used in the calculation of ternary compounds are the same k points from which those of Eq. (2) are generated,⁶⁷ but folded into the smaller ternary Brillouin zone. For the CuAu-I structure these are

$$\mathbf{k}_1 = (2\pi/a)(\frac{1}{4}, \frac{1}{4}, \frac{1}{4}), \quad \omega_1 = \frac{1}{2} \quad (3a)$$

$$\mathbf{k}_2 = (2\pi/a)(\frac{1}{4}, \frac{3}{4}, \frac{1}{4}), \quad \omega_2 = \frac{1}{2} \quad (3b)$$

For the luzonite, famatinite, and chalcopyrite structures, we have

$$\mathbf{k}_1 = (2\pi/a)(\frac{1}{4}, \frac{1}{4}, \frac{1}{4}), \quad \omega_1 = 1 \quad (4)$$

whereas for the CuPt structure the k points equivalent to Eq. (2) are

$$\mathbf{k}_1 = (2\pi/a)(\frac{1}{4}, \frac{1}{4}, \frac{1}{4}), \quad \omega_1 = \frac{1}{16} \quad (5a)$$

$$\mathbf{k}_2 = (2\pi/a)(-\frac{1}{4}, \frac{1}{4}, \frac{1}{4}), \quad \omega_2 = \frac{6}{16} \quad (5b)$$

$$\mathbf{k}_3 = (2\pi/a)(-\frac{1}{4}, \frac{3}{4}, -\frac{1}{4}), \quad \omega_3 = \frac{3}{16} \quad (5c)$$

$$\mathbf{k}_4 = (2\pi/a)(\frac{1}{4}, -\frac{1}{4}, \frac{3}{4}), \quad \omega_4 = \frac{6}{16} \quad (5d)$$

Using the equivalent k points of Eqs. (2)–(5) guarantees that properties calculated for AC or BC in either the zinc-blende structure or in the ternary structures of Fig. 1 will have the same values. Finally, a rapid convergence in the self-consistent iteration is achieved by using Broyden's method, recently adopted for the general potential LAPW calculation.⁶⁸

IV. RESULTS FOR THE BINARY CONSTITUENTS:

AlAs, GaAs, AND GaSb

Before presenting the results for the ternary compounds (Sec. V), we will first establish the reference results for the binary constituents.

A. Structural ground-state properties

Table V compares the calculated equilibrium lattice constants, bulk moduli, and cohesive energies of AlAs, GaAs, and GaSb with the experimental values^{69,70} showing reasonable agreement, considering that the only input to the calculations are atomic numbers of the constituents and the crystal-structure type. The calculated cohesive energies are too large compared to experiment. (In the atomic calculations we have included the spin-polarization energy 0.19, 0.19, 1.58, and 1.35 eV for Al, Ga, As, and Sb, respectively.) That this error is primarily due to the error that use of the LDA entails in the *atomic* total energies can be seen by noting that the cohesive energy *differences* between the three compounds are close to the experimental values. Note that whereas octet solid compounds are "closed shell," the constituent atoms are "open shell," and, hence, distribution of M electrons in their N -fold-degenerate ($N > M$) states gives rise to a series of multiplets. Central-field calculations miss this effect by distributing M/N electrons in each degenerate partner, underestimating⁷¹ the atomic energies.

B. Spin-orbit splittings and deformation potentials

Table VI summarizes the calculated and experimental⁶⁹ spin-orbit (SO) splittings Δ_0 , Δ'_0 , Δ_1 , Δ_2 , and Δ_d at Γ_{15v} , Γ_{15c} , L_{3v} , X_{5v} , and the Ga $3d$ band, respectively, showing good agreement between theory and experiment.

TABLE V. Calculated and experimental values for equilibrium lattice constant a_{eq} , bulk modulus B , and cohesive energy E_c of AlAs, GaAs, and GaSb.

Compound	a_{eq} (Å)		B (GPa)		E_c (eV/2-atoms)	
	Calc.	Expt. ^a	Calc.	Expt. ^a	Calc.	Expt. ^b
AlAs	5.656	5.659	76.1	~77	8.66	7.62
GaAs	5.682	5.652	74.6	75.4	7.81	6.62
GaSb	6.107	6.096	51.8	57.8	7.12	6.00

^aReference 69.

^bReference 70.

Also given are the measured⁶⁹ and calculated pressure deformation potentials dE_g/dp near the equilibrium volumes for the $\Gamma_v \rightarrow \Gamma_{1c}$, $\Gamma_v \rightarrow X_{1c}$, $\Gamma_v \rightarrow X_{3c}$, and $\Gamma_v \rightarrow L_{1c}$ transitions, again demonstrating good agreement between theory and experiment. Our calculated deformation potentials for GaAs are also in good agreement with those calculated by Christensen⁷² and by Chang *et al.*⁷³

The distinction between the conduction states X_{1c} and X_{3c} in zinc-blende semiconductors has often led to considerable confusion in the literature,^{59,74-76} since the designation X_1 and X_3 depends on the choice of origin of the coordinate system⁷⁷ (rarely reported in the literature). When the origin is on the anion site (which is the convention we used in this study) X_{1c} is a cation $p +$ anion s state, and X_{3c} is a anion $p +$ cation s state. Furthermore, since direct optical transitions to X_{1c} and X_{3c} have similar oscillator strengths, it is not trivial to distinguish transitions to these final states in electroreflectance or absorption experiments. Tables I–III further show that this distinction is central to the understanding of the X -derived states in ternary systems, since, for example, in CuAu-I common-anion compounds X_{3c} folds into $\bar{\Gamma}_1$, whereas it is X_{1c} which folds into $\bar{\Gamma}_1$ in common-cation compounds. The symmetry of the X -point states is also important in discussion of the electronic structure of “filled tetrahedral compounds.”⁷⁸ While we distinguish these states on the basis of a symmetry analysis of the

wave functions, our results in Table VI show that they could be distinguished experimentally also on the basis of their widely different deformation potentials. We find that

$$\left| \frac{dE(\Gamma_v - X_{1c})}{dp} \right| \gg \left| \frac{dE(\Gamma_v - X_{3c})}{dp} \right|.$$

Similar results have been found in other III-V and II-VI semiconductor compounds⁷⁹ in the zinc-blende structure. We find that for GaSb the order of the two conduction states at X is different from that found in AlAs and GaAs: the X_{3c} is below the X_{1c} state in GaSb.^{78(b)} This change was missed in previous calculations. Minimal-basis-set tight-binding models^{59,80} predict erroneously that (i) X_{1c} is universally above X_{3c} , and (ii) both states have positive deformation potentials. This is shown in the Appendix.

The different signs of the pressure derivatives for the $\Gamma_{15v} - \Gamma_{1c}$ and $\Gamma_{15v} - X_{1c}$ transitions suggest that at some critical pressure p_c there will be a direct-indirect transition for GaAs and GaSb. Using our calculated pressure derivatives in Table VI and the LDA-corrected zero-pressure direct- and indirect-transition energies (see following discussion and Table XI), we predict that the level crossing occurs around $p_c = 37$ kbar for GaAs and $p_c = 39$ kbar for GaSb. Our result for GaAs is consistent with the photoluminescence measurement of Prins *et al.*,⁸¹

TABLE VI. Calculated and measured spin-orbit splitting Δ (in eV) and deformation potential $a = dE_g/dp$ (in meV/kbar) of some fundamental band states of AlAs, GaAs, and GaSb. For GaAs and GaSb we use the Ceperley-Alder exchange-correlation potential (Ref. 64), whereas for AlAs we use the Hedin-Lundqvist formula (Ref. 65).

Property	AlAs		GaAs		GaSb	
	Calc.	Expt. ^a	Calc.	Expt. ^a	Calc.	Expt. ^a
Δ_0 (Γ_{15v})	0.303	0.28	0.338	0.34	0.708	0.75
Δ'_0 (Γ_{15c})	0.03		0.19	0.17	0.22	0.21
Δ_1 (L_{3v})	0.18	0.20	0.21	0.22	0.40	0.43
Δ_2 (X_{5v})	0.13	0.15	0.08	0.08	0.24	0.24
Δ_d (Γ_d)			0.46	0.45	0.46	0.45
a ($\Gamma_{15v} - \Gamma_{1c}$)	10.6		10.3	8.5–12.6	14.3	14.8
a ($\Gamma_{15v} - X_{1c}$)	–2.2		–2.2	–2.7 to –1.8	–3.4	
a ($\Gamma_{15v} - X_{3c}$)	0.2		–0.3		–1.8	
a ($\Gamma_{15v} - L_{1c}$)	5.1		3.9	5.5	4.3	5

^aReference 69.

TABLE VII. Calculated semirelativistic LDA band energies at some high-symmetry points (in eV). For AlAs the Hedin-Lunqvist (HL) exchange-correlation formula (Ref. 65) is used, whereas for GaAs and GaSb the Ceperley-Alder (CAD) form (Ref. 64) is used. Results for GaAs indicate that the difference between the results obtained from these two functions are <0.01 eV. All results are calculated at the respective experimental lattice constants (Table V).

State	AlAs a_{expt} (HL)	GaAs a_{expt} (CAD)	GaSb a_{expt} (CAD)
Γ_{1v}	-11.93	-12.77	-11.61
Γ_{15v}	0	0	0
Γ_{1c}	1.85	0.24	-0.13
Γ_{15c}	4.23	3.65	2.75
X_{1v}	-9.97	-10.37	-9.17
X_{3v}	-5.47	-6.91	-6.92
X_{5v}	-2.19	-2.69	-2.61
X_{1c}	1.31	1.32	1.14
X_{3c}	2.18	1.53	0.81
L_{1v}	-10.51	-11.10	-10.00
L_{1v}	-5.62	-6.71	-6.47
L_{3v}	-0.83	-1.15	-1.17
L_{1c}	2.00	0.81	0.28
L_{3c}	4.62	4.56	3.72
W_{1v}	-9.92	-10.34	-9.15
W_{3v}	-5.11	-6.72	-6.80
W_{4v}	-3.21	-3.57	-3.42
W_{2v}	-2.85	-3.37	-3.20
W_{3c}	5.57	4.51	3.63
W_{2c}	4.25	4.63	4.26
W_{1c}	5.62	5.27	4.34
W_{4c}	5.97	5.94	4.70

who find $p_c=41$ kbar at room temperature, and it is larger than the calculated result of Christensen⁷² (~ 31 kbar).

C. LDA band energies and corrections

Table VII gives the LDA band energies (evaluated at the experimental lattice parameters of Table V) for AlAs,

GaAs, and GaSb. Table VIII contrasts the LDA-calculated band energies, at the theoretical equilibrium lattice parameters with the low-temperature experimental band gaps.⁸² In contrast with the good agreement obtained for various ground-state properties (Tables V and VI), Table VIII demonstrates the well-known^{64(a)} underestimation of the experimental gaps by LDA eigenvalue differences. The calculated Ga 3d levels at $\epsilon_v - 15$ eV are also found to be about 4 eV higher than the experimental photoemission values.⁸³ This is expected since relaxation effects (which tend to lower the Ga 3d level) are not included in the band calculation.⁸⁴

Although much of the work described in what follows concentrates on contrasting the *relative* band gaps of ternary and binary compounds at the same compositions (hence, LDA errors can be expected to partially cancel), it is desirable to systematically correct the LDA error so that a direct comparison between the calculated and experimental gaps is possible. This will be done as follows. First, we establish the correction $\delta_{m,k}$ to the LDA band gaps of band m and wave vector k in the binary compounds (Table VIII). Second, we establish for each wave function of the ternary $A_nB_{4-n}C_4$ structures its projection onto the states $|AC,m,k\rangle$ and $|BC,m,k\rangle$ of the binary constituents. This identification is aided by the folding relationships between states in the ternary and binary phases (Tables I–III). Third, we apply to each state in the ternary compound the corrections $\{\delta_{m,k}\}$ of the binary constituents, weighted according to their proportion in the wave functions. Given the fact that the LDA corrections $\delta_{m,k}$ for a given (m,k) are rather similar for different binary compounds (Table VIII), this procedure is expected to introduce but a small error. The LDA-corrected results will be displayed in Table X below.

V. RESULTS FOR ORDERED TERNARY COMPOUNDS

A. Structural ground-state properties of the ternary systems

Before performing band-structure calculations on the ordered ternary phases, their equilibrium structural pa-

TABLE VIII. Calculated and experimental values for conduction- and valence-band energies (in eV) of GaAs and GaSb (relative to the valence-band maximum). Spin-orbit splittings of X_{5v} and L_{3v} states are neglected. The LDA energy levels are obtained at the calculated (calc) lattice constants (Table V).

State	AlAs			GaAs			GaSb		
	LDA a_{calc} (HL)	Expt. ^a	Diff.	LDA a_{calc} (CAD)	Expt. ^a	Diff.	LDA a_{calc} (CAD)	Expt. ^a	Diff.
VBM	0	0	0	0	0	0	0	0	0
Γ_{1c}	1.84	3.13	1.29	0.15	1.52	1.37	-0.165	0.81	0.98
X_{5v}	-2.19	-2.41	-0.22	-2.63	-2.92	-0.29	-2.58	-2.94	-0.36
X_{1c}	1.32	2.23	0.91	1.36	1.98	0.62	1.16	1.66	0.50
X_{3c}	2.18	2.99	0.81	1.55	2.30	0.75	0.83	1.43	0.60
L_{3v}	-0.83	-1.12	-0.29	-1.12	-1.41	-0.29	-1.16	-1.33	-0.17
L_{1c}	1.99	3.03	1.04	0.79	1.81	1.02	0.28	1.09	0.81

^aReference 82.

rameters need to be established through total-energy minimization. In addition to the unit-cell lattice vectors, the ternary $A_nB_{4-n}C_4$ structures of Fig. 1 have cell-internal structural parameters which determine the equilibrium bond lengths R_{A-C} and R_{B-C} and the bond angles. We have minimized for $\text{Ga}_4\text{As}_n\text{Sb}_{4-n}$ the total energy of each of the ordered structures, with respect to both the unit-cell lattice parameters and the cell-internal degrees of freedom. The resulting equilibrium structural parameters are given in Table IX. We see that the cubic lattice constants of these ordered compounds follow closely Vegard's rule,⁸⁵ i.e., $a_{\text{eq}}^{(n)} \simeq \frac{1}{4}[na_{\text{eq}}(AC) + (4-n)a_{\text{eq}}(BC)]$. In contrast, bond lengths do not average, but instead exhibit a bimodal distribution^{12,86} whereby the Ga—As and Ga—Sb bond lengths in the ternary compounds are closer to their respective ideal bond lengths in the binary constituents than to the averaged bond length $\bar{R}^{(n)} = \sqrt{3}/4a_{\text{eq}}^{(n)}$. This indicates that the system has used its cell-internal degree of freedom to minimize its strain energy associated with size mismatches.

Since the experimental and calculated lattice mismatch between GaAs and AlAs is small, we have assumed an averaged lattice constant $a = 5.6569 \text{ \AA}$ with equal Ga—As and Al—As bond lengths for the $\text{Al}_n\text{Ga}_{4-n}\text{As}_4$ system.

B. Valence-band offset in GaAs/GaSb

The extent to which given wave functions in $A_nB_{4-n}C_4$ are preferentially localized on a given sublattice reflects the relative alignments of AC -derived and BC -derived energy levels. It is, hence, useful to first establish this alignment at the limit of *thick* AC and BC layers, i.e., the band offsets. We have previously proposed a method⁸⁷ to calculate the valence-band offset ΔE_v in a way that parallels its measurement in photoemission

core-level spectroscopy.⁸⁸ In this approach, we need to know the core- (n,l) level binding energies $\epsilon_{nl,A}^{AC}$ and $\epsilon_{nl,B}^{BC}$ for the binaries AC and BC with respect to their respective valence-band maxima, and the core-level difference $\Delta\epsilon_{nl,n'l'}^{AC,BC}$. This method has been successfully used to calculate ΔE_v for GaAs/AlAs and some II-VI compound common anion pairs.^{87,89} Here we apply this method to estimate ΔE_v for the GaAs/GaSb system. The core-level binding energies $\epsilon_{1s,\text{As}}^{\text{GaAs}}$ and $\epsilon_{1s,\text{Sb}}^{\text{GaSb}}$ are obtained from the binary band-structure calculation. The core-level binding-energy difference $\Delta\epsilon_{1s,1s}^{\text{As,Sb}}$ can be obtained from calculations for Ga_2AsSb in either the CuAu, CuPt, or chalcopyrite structures; the values agree to within 0.1 eV. Using these results we find $\Delta E_v(\text{GaAs/GaSb}) \approx 0.65 \pm 0.10 \text{ eV}$, where the contribution $\frac{1}{3}[\Delta_0(\text{GaSb}) - \Delta_0(\text{GaAs})] = 0.12 \text{ eV}$ from the spin-orbit splitting has been included. Our results compare well with those we calculated using the tight-binding method⁹⁰ (0.58 eV). No direct experimental value is available for comparison. The experimental value⁹¹ for InAs/GaSb and GaAs/InAs pairs are 0.46 and 0.17 eV, respectively. Assuming ΔE_v to be transitive,⁹² we estimate the experimental value to be their sum, i.e., 0.63 eV, in good agreement with our calculated value.

Using our calculated band offset and the (LDA-corrected) energy levels of the binary constituents (Table VIII), we can now place them on an absolute energy scale. Figures 5(a) and 5(b) show the results for GaAs-GaSb; a similar figure for GaAs-AlAs was given in Ref. 25. Figure 5 shows that the valence-band maximum is on the GaSb side. The conduction states Γ_{1c} , L_{1c} , and X_{3c} likewise have their well minima on the GaSb sublattice, whereas the X_{1c} state has its well minimum on the GaAs sublattice. The conduction-band offsets are 0.06, 0.07, -0.33 , and 0.22 eV for Γ_{1c} , L_{1c} , X_{1c} , and X_{3c} , respec-

TABLE IX. Calculated equilibrium lattice constants a_{eq} , cell-internal relaxation parameters $\{u_{\text{eq}}\}$, and Ga—As and Ga—Sb bond lengths for various ordered Ga(As,Sb) structures (shown in Fig. 1). The numbers in the parentheses are the weight of different bonds in the unit cell. For details of the notation, see Ref. 19.

Formula	Structure	a_{eq} (\AA)	$\{u_{\text{eq}}\}$	$R_{\text{Ga-Sb}}$ (\AA)	$R_{\text{Ga-As}}$ (\AA)
Ga_4Sb_4	zinc-blende	6.1068	0.25	2.6443	
Ga_4AsSb_3	luzonite	6.0071	0.2417	2.6313	2.5146
Ga_4AsSb_3	famatinite	6.0046	$u = 0.2404$ $2v = 0.2423$	$2.6413 (\times 1)$ $2.6283 (\times 2)$	2.5068
$\text{Ga}_4\text{As}_2\text{Sb}_2$	CuAu-I	5.8927	0.2336	2.6085	2.4971
$\text{Ga}_4\text{As}_2\text{Sb}_2$	chalcopyrite	5.8922	0.2294	2.6233	2.4833
$\text{Ga}_4\text{As}_2\text{Sb}_2$	CuPt	5.8974	$u1 = 0.2410$ $u2 = 0.2590$	$2.5857 (\times 3)$ $2.6456 (\times 1)$	$2.4617 (\times 1)$ $2.5245 (\times 3)$
$\text{Ga}_4\text{As}_3\text{Sb}$	luzonite	5.7852	0.2579	2.5844	2.4797
$\text{Ga}_4\text{As}_3\text{Sb}$	famatinite	5.7823	$u = 0.2604$ $2v = 0.2584$	2.6013	$2.4640 (\times 1)$ $2.4776 (\times 2)$
Ga_4As_4	zinc-blende	5.6816	0.25		2.4602

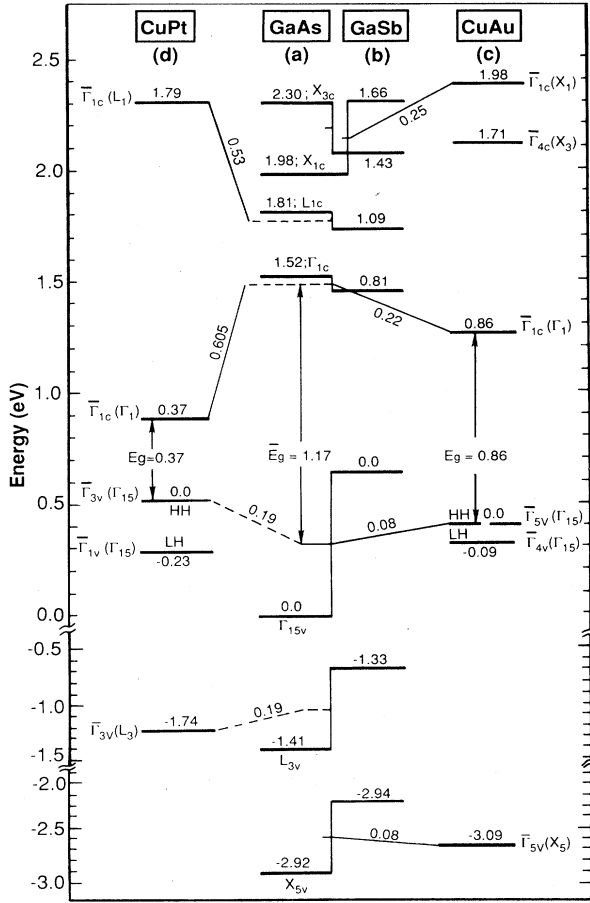


FIG. 5. (a) and (b) show the energy levels of GaAs and GaSb, placed on a common energy scale (obtained from the calculated valence-band offset). (c) and (d) show the energy levels of Ga_2AsSb in the CuAu-I and CuPt structure, respectively. Note how level repulsion displaces in (c) the $\{\bar{\Gamma}_{5v}(\Gamma_{15v}); \bar{\Gamma}_{5v}(X_{5v})\}$ and the $[\bar{\Gamma}_{1c}(\bar{\Gamma}_{1c}); \bar{\Gamma}_{1c}(X_{1c})]$ pairs relative to their well centers. A stronger effect is seen in (d) for the CuPt structure, where $\{\bar{\Gamma}_{3v}(L_{3v}); \bar{\Gamma}_{3v}(\Gamma_{15v})\}$ and $\{\bar{\Gamma}_{1c}(\Gamma_1); \bar{\Gamma}_{1c}(L_1)\}$ are strongly shifted.

tively. We have also indicated in Fig. 5 the position of the “well centers” (average energies of the binaries) for each of the states.

This analysis has the following relevance to our present discussion. In an $(AC)_n(BC)_n$ superlattice, the states can be classified as “mass delocalized” (when the effective mass is sufficiently small) or “mass localized” (when the effective mass is sufficiently heavy and the barrier height sufficiently large). Wave functions of mass-delocalized states are extended on both sublattices and their energies are near the well center. Mass-localized states have their energies between the well center and the well edge; their wave functions are preferentially localized on the sublattice corresponding to the well edge. Since some of the ordered $A_nB_{4-n}C_4$ structures considered here are in fact superlattices (e.g., CuAu is (1,1) superlattice along the [001] direction and CuPt is a (1,1) superlattice along the

[111] direction; see Fig. 1), we will compare their energy levels to the well-center and well-bottom energies of Fig. 5, to discuss wave-function localization. Note that for lattice-mismatched system like Ga(As,Sb), the energy alignment of Fig. 5 pertinent to thick superlattices will be modified for ultrathin superlattice, particularly for those conduction states which are sensitive to the bond-length variation. However, the centers of the quantum wells are not sensitive to the bond-length variation for Ga(As,Sb) since their deformation potentials dE_g/da are quite similar.⁶⁹

C. Optical bowing in ordered ternary compounds and its analyses

In analogy with the common convention in *disordered* alloys,⁵¹ we can define optical bowing parameters for the $i \rightarrow j$ interband transition in *ordered* compound of structure α as

$$\epsilon^{(ij,\alpha)}(X_n) = \bar{\epsilon}^{(ij)}(X_n) - b^{(ij,\alpha)}X_n(1 - X_n), \quad (6)$$

where $\bar{\epsilon}^{(ij)}$ is the linear composition-weighted energy for the $i \rightarrow j$ transitions in the binary constituents,

$$\bar{\epsilon}^{(ij)}(X_n) = X_n \epsilon_{AC}^{(ij)} + (1 - X_n) \epsilon_{BC}^{(ij)}, \quad (7)$$

and $X_n = n/4$ is the composition of AC in the structure $A_nB_{4-n}C_4$. For the 50%-50% structures $b^{(ij,\alpha)}$ is simply $4(\bar{\epsilon} - \epsilon)$.

To better understand the physical content of the bowing parameter $b^{(ij,\alpha)}$, we have decomposed it, following Refs. 22 into three physically recognizable contributions. Consider the three-step process of forming, say, ordered ABC_2 from $AC + BC$.

(i) Compress and dilate AC and BC from their respective equilibrium volumes V_{AC} and V_{BC} to the volume V_{ABC_2} of the ternary ordered structure. The attendant volume-deformation (VD) contribution to the bowing parameter is

$$b_{VD}^{(ij)} = 2[\epsilon_{AC}^{(ij)}(V_{AC}) - \epsilon_{AC}^{(ij)}(V_{ABC})] + 2[\epsilon_{BC}^{(ij)}(V_{BC}) - \epsilon_{BC}^{(ij)}(V_{ABC})]. \quad (8)$$

No level-repulsion mechanism is involved in b_{VD} ; its value reflects the AC and BC deformation potentials. Since the equilibrium lattice constants of the ternary compounds usually follow Vegard's rule, b_{VD} is expected to be small if the deformation potentials dE_g/da of the binary constituents are similar (or, if dE_g/dp of the constituent with larger lattice constant is larger).

(ii) Bring together AC and BC, already prepared at the volume V_{ABC} , to form the ternary ABC phase; however, keep this ternary phase unrelaxed at its ideal $\{u_0\}$ structure parameters. The corresponding contribution of this charge-exchange (CE) term to the bowing is

$$b_{CE}^{(ij,\alpha)} = 2\epsilon_{AC}^{(ij)}(V_{ABC}) + 2\epsilon_{BC}^{(ij)}(V_{ABC}) - 4\epsilon_{ABC}^{(ij,\alpha)}(V_{ABC}, \{u_0^{(\alpha)}\}). \quad (9)$$

This term isolates the effect of the piece of the ordering potential which reflects chemical differences between A

and B .

(iii) Let the ternary structure relax to its energy-minimizing geometry through adjustments in the structural parameters $\{u\}$ (Table IX) to their equilibrium (eq) values $\{u_{eq}\}$. The structural (S) contribution to the bowing is

$$b_S^{(ij,\alpha)} = 4\epsilon_{ABC}^{(ij,\alpha)}(V_{ABC}, \{u_0\}) - 4\epsilon_{ABC}^{(ij,\alpha)}(V_{ABC}, \{u_{eq}\}). \quad (10)$$

Summing Eqs. (11)–(13), we find the total bowing parameter,

$$b^{(ij,\alpha)} = b_{VD}^{(ij)} + b_{CE}^{(ij,\alpha)} + b_S^{(ij,\alpha)} \\ = 2\epsilon_{AC}^{(ij)}(V_{AC}) + 2\epsilon_{BC}^{(ij)}(V_{BC}) - 4\epsilon_{ABC}^{(ij,\alpha)}(V_{ABC}, \{u_{eq}\}), \quad (11)$$

just as in the defining Eqs. (6) and (7). We will present some calculated values for the components of b to establish the relative significance of the three underlying effects in these systems.

Table X gives the calculated LDA $\bar{\Gamma}_v \rightarrow \bar{\Gamma}_{1c}$ band gaps of the ternary systems and the LDA-corrected values, using the procedure described in Sec. IV C. Tables XI and XII give the LDA and LDA-corrected results for other $\bar{\Gamma}$ -folded conduction bands in the 50%-50% ordered Ga_2AsSb and GaAlAs_2 , respectively. Table XIII gives $b^{(ij,\alpha)}$ for the direct band gap $\bar{\Gamma}_v \rightarrow \bar{\Gamma}_{1c}$ (Γ_{1c}) as well as for the spin-orbit splitting $b^{(\alpha)}(\Delta_0)$ at the valence-band maximum for all seven ordered structures α .

In the following subsections we present a detailed analysis for the ordered structures.

D. Electronic structure of ordered GaAs-GaSb compounds

Figure 6 depicts the LDA-corrected energy levels at $\bar{\Gamma}$ of $\text{Ga}_4\text{As}_2\text{Sb}_2$ in the CuAu-I-like, chalcopyrite, and CuPt-like structures, along with the levels of the binary constituents which fold into these states. Table XIV gives an angular-momentum analysis of the wave functions at $\bar{\Gamma}$. These results can be discussed in terms of the physical principles underlined in Sec. II.

1. CuAu-I

Figure 6(a) shows the energy levels of this system relative to the common valence band, whereas Fig. 5(c) shows the results relative to the energy levels of the binary constituents, on an absolute energy scale.

The first repelling pair is $\{\bar{\Gamma}_{5v}(X_{5v}); \bar{\Gamma}_{5v}(\Gamma_{15v})\}$, showing energy shifts of ± 0.085 eV relative to the respective well centers. Due to the valence-band offset between GaAs and GaSb (maximum on GaSb) and the upward repulsion of $\bar{\Gamma}_{5v}(\Gamma_{15v})$, we expect this state to show a preferential localization on the GaSb sublattice. Figures 7 and 8 show the calculated electronic charge densities at the valence-band maximum (VBM) in GaSb and GaAs, respectively, whereas Fig. 9 shows the corresponding results for Ga_2AsSb in the CuAu-I-like structure (all calculated at their respective theoretical lattice constants, Table V), confirming this expectation. The crystal-field splitting $\bar{\Gamma}_{5v} - \bar{\Gamma}_{4v}$ is ~ 0.09 eV. Whereas the $\bar{\Gamma}_{4v}$ state has a higher (p -like) amplitude on As [Fig. 9(c)], the $\bar{\Gamma}_{5v}$ state has a larger amplitude on Sb. This reflects the fact that level repulsion displaced the $\bar{\Gamma}_{5v}$ state to *higher* energies, and, hence, closer to the GaSb well maximum.

The next pair of repelling states is $\{\bar{\Gamma}_{1c}(\Gamma_{1c}); \bar{\Gamma}_{1c}(X_{1c})\}$, exhibiting substantial ($\sim \pm 0.24$ eV) energy shifts. Figures 9(a) shows that this leads to a preferential localization of the $\bar{\Gamma}_{1c}(\Gamma_{1c})$ wave function on the As sublattice,⁹³ since As has a deeper 4s orbital than the 5s orbital of Sb (see Table IV).

The upwards shift of the $\bar{\Gamma}_{5v}$ VBM (by 0.085 eV) and the downward shift of the $\bar{\Gamma}_{1c}$ conduction-band minimum (by 0.223 eV) leads to a gap reduction by 0.308 eV, and, hence, a bowing parameter of 1.23 eV.

2. Chalcopyrite

The energy levels near the band edge at $\bar{\Gamma}$ for this structure [Fig. 6(b)] are very close to the concentration-averaged values (i.e., very small bowing). The reason for this is that the repulsions between $\bar{\Gamma}_{1c}(\Gamma_{1c})$ and $\bar{\Gamma}_{1c}(W_{1c})$ and that between $\bar{\Gamma}_{5v}(\Gamma_{15v})$ and $\bar{\Gamma}_{5v}(W_{2v})$ [out-

TABLE X. Fundamental direct band gaps (in eV) derived from the zinc-blende ($\Gamma_{15v} - \Gamma_{1c}$) transition of $\text{Ga}_4\text{As}_n\text{Sb}_{4-n}$ and $\text{Al}_n\text{Ga}_{4-n}\text{As}_4$ before and after LDA correction. Results for $\text{Ga}_4\text{As}_n\text{Sb}_{4-n}$ are calculated at the theoretical lattice constants (see Table IX); those for $\text{Al}_n\text{Ga}_{4-n}\text{As}_4$ are calculated at $a = 5.6569$ Å.

Compound	Structure	LDA (CAD)	LDA corrected	Compound	LDA (HL)	LDA corrected
		a_{calc}			a_{expt}	
Ga_4As_4	zinc-blende	0.154	1.52	Ga_4As_4	0.241	1.52
$\text{Ga}_4\text{As}_3\text{Sb}$	luzonite	-0.175	1.09	AlGa_3As_4	0.601	1.89
$\text{Ga}_4\text{As}_3\text{Sb}$	famatinite	-0.054	1.22	AlGa_3As_4	0.633	1.92
$\text{Ga}_4\text{As}_2\text{Sb}_2$	CuAu-I	-0.316	0.86	$\text{Al}_2\text{Ga}_2\text{As}_4$	0.893	2.18
$\text{Ga}_4\text{As}_2\text{Sb}_2$	chalcopyrite	-0.050	1.13	$\text{Al}_2\text{Ga}_2\text{As}_4$	1.068	2.36
$\text{Ga}_4\text{As}_2\text{Sb}_2$	CuPt	-0.781	0.37	$\text{Al}_2\text{Ga}_2\text{As}_4$	0.683	1.97
Ga_4AsSb_3	luzonite	-0.290	0.79	Al_3GaAs_4	1.144	2.43
Ga_4AsSb_3	famatinite	-0.170	0.91	Al_3GaAs_4	1.377	2.66
Ga_4Sb_4	zinc-blende	-0.165	0.81	Al_4As_4	1.849	3.13

TABLE XI. LDA and LDA-corrected band energies with respect to the valence-band maximum (in eV) of the three ordered $\text{Ga}_4\text{As}_2\text{Sb}_2$ structures at $\bar{\Gamma}$.

ZB label	$\text{Ga}_4\text{As}_2\text{Sb}_2$ (CA)			$\text{Ga}_4\text{As}_2\text{Sb}_2$ (CH)			$\text{Ga}_4\text{As}_2\text{Sb}_2$ (CP)		
	State	LDA	LDA corrected	State	LDA	LDA corrected	State	LDA	LDA corrected
Γ_{15v}	$\bar{\Gamma}_{5v}$	0.0 ^a	0.0 ^a	$\bar{\Gamma}_{5v}$	-0.01	-0.01	$\bar{\Gamma}_{3v}$	0.0 ^a	0.0 ^a
Γ_{15v}	$\bar{\Gamma}_{4v}$	-0.09	-0.09	$\bar{\Gamma}_{4v}$	0.0 ^a	0.0 ^a	$\bar{\Gamma}_{1v}$	-0.23	-0.23
Γ_{1c}	$\bar{\Gamma}_{1c}$	-0.316	0.86	$\bar{\Gamma}_{1c}$	-0.050	1.13	$\bar{\Gamma}_{1c}$	-0.781	0.37
X_{5v}	$\bar{\Gamma}_{5v}$	-2.76	-3.09	$\bar{\Gamma}_{5v}$	-2.57	-2.90			
X_{1c}	$\bar{\Gamma}_{1c}$	1.42	1.98	$\bar{\Gamma}_{3c}$	1.23	1.79			
X_{3c}	$\bar{\Gamma}_{4c}$	1.03	1.71	$\bar{\Gamma}_{2c}$	1.14	1.82			
L_{3v}							$\bar{\Gamma}_{3v}$	-1.51	-1.74
L_{1c}							$\bar{\Gamma}_{1c}$	-0.90	-1.79

^aValence-band maximum.TABLE XII. LDA and LDA-corrected band energies with respect to the valence-band maximum (in eV) of the three ordered $\text{Al}_2\text{Ga}_2\text{As}_4$ structures at $\bar{\Gamma}$.

ZB label	$\text{Al}_2\text{Ga}_2\text{As}_4$ (CA)			$\text{Al}_2\text{Ga}_2\text{As}_4$ (CH)			$\text{Al}_2\text{Ga}_2\text{As}_4$ (CP)		
	State	LDA	LDA corrected	State	LDA	LDA corrected	State	LDA	LDA corrected
Γ_{15v}	$\bar{\Gamma}_{5v}$	0.0 ^a	0.0 ^a	$\bar{\Gamma}_{5v}$	-0.01	-0.01	$\bar{\Gamma}_{3v}$	0.0 ^a	0.0 ^a
Γ_{15v}	$\bar{\Gamma}_{4v}$	-0.05	-0.05	$\bar{\Gamma}_{4v}$	0.0 ^a	0.0 ^a	$\bar{\Gamma}_{1v}$	-0.03	-0.03
Γ_{1c}	$\bar{\Gamma}_{1c}$	0.893	2.18	$\bar{\Gamma}_{1c}$	1.068	2.36	$\bar{\Gamma}_{1c}$	0.683	1.97
X_{5v}	$\bar{\Gamma}_{5v}$	-2.44	-2.66	$\bar{\Gamma}_{5v}$	-2.44	-2.66			
X_{1c}	$\bar{\Gamma}_{4c}$	1.38	2.17	$\bar{\Gamma}_{2c}$	1.31	2.10			
X_{3c}	$\bar{\Gamma}_{1c}$	2.04	2.83	$\bar{\Gamma}_{3c}$	1.78	2.57			
L_{3v}							$\bar{\Gamma}_{3v}$	-1.00	-1.28
L_{1c}							$\bar{\Gamma}_{1v}$	1.81	2.83

^aValence-band maximum.TABLE XIII. Calculated bowing coefficient and spin-orbit splitting (all in eV) of ordered $\text{Ga}_4\text{As}_n\text{Sb}_{4-n}$ and $\text{Al}_n\text{Ga}_{4-n}\text{As}_4$. Results for $\text{Ga}_4\text{As}_n\text{Sb}_{4-n}$ are calculated at the theoretical lattice constant using the CAD correlation potential (Ref. 64). Results for $\text{Al}_n\text{Ga}_{4-n}\text{As}_4$ are calculated at $a = 5.6569 \text{ \AA}$ using the HL correlation potential (Ref. 65). $\text{Al}_{4-n}\text{Ga}_n\text{As}_4$ has zero bowing of the spin-orbit splitting Δ_0 .

Structure	Compound	b_n			b_n		
		$\bar{\Gamma}_v \rightarrow \bar{\Gamma}_{1c}$	Δ_0 a_{calc}	Δ_0 a_{calc}	Compound	$\bar{\Gamma}_v \rightarrow \bar{\Gamma}_{1c}$	b_n $\bar{\Gamma}_v \rightarrow \bar{\Gamma}_{1c}$
luzonite	$\text{Ga}_4\text{As}_3\text{Sb}$	1.31	0.453	-0.12	AlGa_3As_4	0.22	
famatinite	$\text{Ga}_4\text{As}_3\text{Sb}$	0.67	0.441	-0.06	AlGa_3As_4	0.05	
CuAu	$\text{Ga}_4\text{As}_2\text{Sb}_2$	1.23	0.549	-0.10	$\text{Al}_2\text{Ga}_2\text{As}_4$	0.61	
chalcopyrite	$\text{Ga}_4\text{As}_2\text{Sb}_2$	0.17	0.521	-0.01	$\text{Al}_2\text{Ga}_2\text{As}_4$	-0.09	
CuPt	$\text{Ga}_4\text{As}_2\text{Sb}_2$	3.18	0.605	-0.33	$\text{Al}_2\text{Ga}_2\text{As}_4$	1.45	
luzonite	Ga_4AsSb_3	1.09	0.630	-0.08	Al_3GaAs_4	1.62	
famatinite	Ga_4AsSb_3	0.45	0.626	-0.06	Al_3GaAs_4	0.37	

TABLE XIV. Calculated l -decomposed electron charges (in percent) inside the muffin-tin (MT) spheres of GaSb, GaAs, Ga₂AsSb (CH), Ga₂AsSb (CA), and Ga₂AsSb (CP) at the radii (in a.u.) $R_{\text{MT}}(\text{Ga}) = 2.3548$, $R_{\text{MT}}(\text{As}) = R_{\text{MT}}(\text{Sb}) = 2.2741$. All the states are normalized to $2e/4$ -atoms cell. Electrons not included inside the MT spheres are in the interstitial regions. We use the MT-sphere

[illegible]

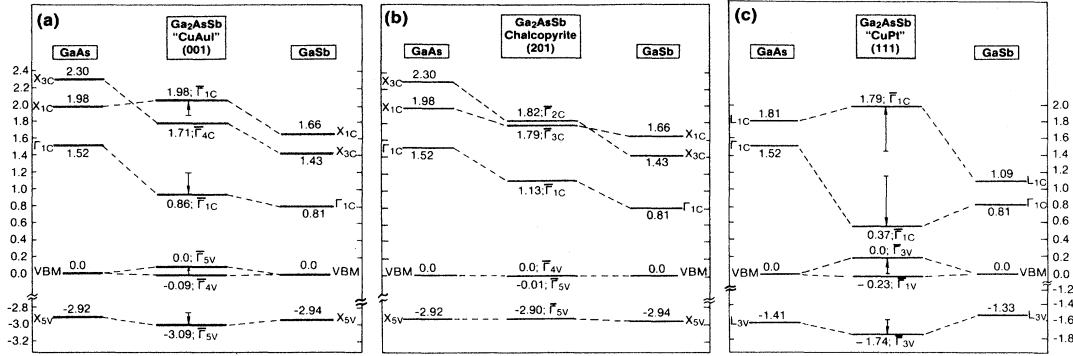


FIG. 6. LDA-corrected energy levels at $\bar{\Gamma}$ of Ga_2AsSb in the (a) CuAu-I-like, (b) chalcopyrite, and (c) CuPt-like structures. Dashed lines connect folding states. Arrows depict the magnitude of the repulsion from the well centers.

side the energy range of Fig. 6(b)] are weak due to large energy denominators: the $\langle W_{1c} \rangle - \langle \Gamma_{1c} \rangle$ and $\langle \Gamma_{15v} \rangle - \langle W_{2v} \rangle$ energy denominators (4.75 and 3.29 eV, respectively) are considerably larger than the corresponding values in the CuAu-I structure $\langle X_{1c} \rangle - \langle \Gamma_{1c} \rangle = 1.18$ eV and $\langle \Gamma_{15v} \rangle - \langle X_{5v} \rangle = 2.65$ eV. The $\bar{\Gamma}_{1c}$ (Γ_{1c}) state is not affected by the folding $\bar{\Gamma}(X_c)$ states since they have different symmetries (Table II). The coupling between $\bar{\Gamma}_{5v}$ (Γ_{5v}) and $\bar{\Gamma}_{5v}$ (X_{5v}) is also weak because the phase factor between Γ and X states is not in good registry with the ordering potential (see Sec. II B). We see that for this structure the $\bar{\Gamma}_{4v}$ (Γ_{15v}) state is above the $\bar{\Gamma}_{5v}$ (Γ_{15v}) state by ~ 0.01 eV, possibly due to the coupling between these states and $\bar{\Gamma}$ (W) states which exist both below and above $\bar{\Gamma}$ (Γ_{15v}) states. This leads to an *inverted* valence

band. No substantial charge localization is found in this structure (Fig. 10).

3. CuPt

Figure 6(c) shows the energy levels of this structure relative to the common VBM, whereas Fig. 5(d) shows the results relative to the energies of the binaries, all placed on an absolute energy scale.

The first repelling pair is $\{\bar{\Gamma}_{3v} (L_{3v}); \bar{\Gamma}_{3v} (\Gamma_{15v})\}$, whose energy shifts are ± 0.19 eV relative to the respective well centers. This upward shift of the $\bar{\Gamma}_{3v}$ VBM substantially enhances its amplitude on the Sb sublattice [Fig. 11(b)] and leads to a large (0.23 eV) crystal-field splitting. The next $\{\bar{\Gamma}_{1c} (\Gamma_{1c}); \bar{\Gamma}_{1c} (L_{1c})\}$ repelling pair shows an enormous shift of ~ 0.60 eV due to the very

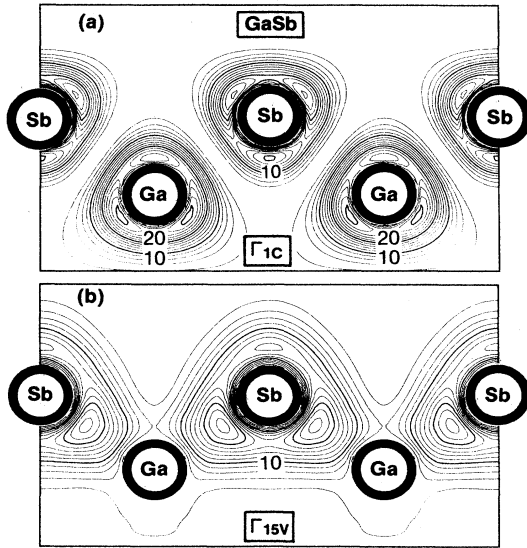


FIG. 7. Electronic charge-density contour plot of GaSb on the (110) plane (in units of $10^{-3} e/a.u.^3$) for (a) the $\bar{\Gamma}_{1c}$ state and (b) the $\bar{\Gamma}_{15v}$ state. The charge for each state has been normalized to be 2 electrons per 2-atom unit cell. The step size of the contour is 2.

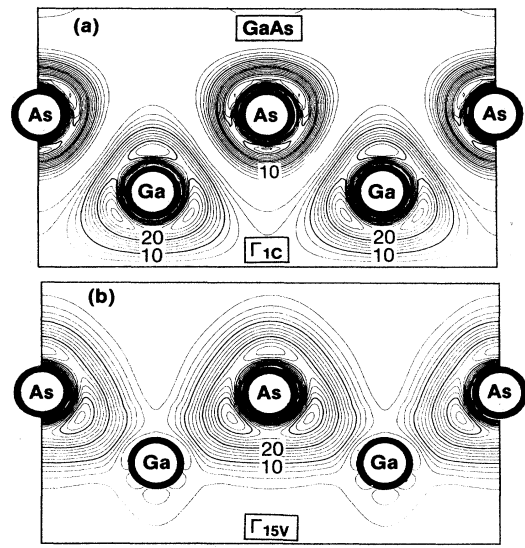


FIG. 8. Electronic charge-density contour plot of GaAs on the (110) plane (in units of $10^{-3} e/a.u.^3$) for (a) the $\bar{\Gamma}_{1c}$ state and (b) the $\bar{\Gamma}_{15v}$ state. The charge for each state has been normalized to be 2 electrons per 2-atom unit cell. The step size of the contour is 2.

small $\langle L_{1c} \rangle - \langle \Gamma_{1c} \rangle$ energy denominator of 0.49 eV. Hence, the $\bar{\Gamma}_{1c}$ (Γ_{1c}) wave-function amplitude is enhanced significantly on the GaAs sublattice [Fig. 11(a)]. This leads to “indirectness in real space” whereby the $\bar{\Gamma}_{3v}$ VBM is localized preferentially on GaSb, whereas the $\bar{\Gamma}_{1c}$ CBM is localized on the GaAs sublattice.

The upward shift of the VBM (by 0.19 eV) and the downward shift of the CBM (by 0.605 eV) leads to a very large bowing coefficient of $4(0.19 + 0.605) = 3.18$ eV. The large crystal-field splitting leads to different localization patterns: while the $\bar{\Gamma}_{3v}$ (Γ_{15v}) state [Fig. 11(b)] is localized preferentially on Sb, the $\bar{\Gamma}_{1v}$ (Γ_{15v}) state [Fig. 11(c)] has a preferred localization on As. Compared with the binaries, the total charge density at the VBM [Fig. 11(d)] is, however, more localized on Sb.

4. General trend for bowing in ordered GaSb-GaAs compounds

We see that because of the different identities of the repelling states and the different symmetry properties, the

bowing coefficients for $\text{Ga}_4\text{As}_n\text{Sb}_{4-n}$ depend strongly on the crystal structure with $b(\text{CP}) > b(\text{CA}) > b(\text{CH})$. Similarly, we find $b(\text{L}) > b(\text{F})$ for $n=1,3$ luzonite and famatinite structures. In all cases we find that the top of valence band at Γ tends to localize on the Sb sublattice and that the bottom of conduction band tends to localize on the As sublattice.

Since the differences $\langle \Gamma_{1c} \rangle - \langle X_{1c} \rangle$ and $\langle \Gamma_{1c} \rangle - \langle L_{1c} \rangle$ in the average energies (Fig. 3) as well as $\langle \Gamma_{15v} \rangle - \langle X_{5v} \rangle$ and $\langle \Gamma_{15v} \rangle - \langle L_{3v} \rangle$ depend on composition weakly and linearly, we find that $b(X_n)$ is only weakly composition dependent for the structures with the (0,0,1) ordering vector (i.e., the ordered CuAu-I-like and “luzonite”-like structures). We find that $b(X_n)$ is slightly larger in As-rich compounds since the energy difference $\langle \Gamma_{1c} \rangle - \langle X_{1c} \rangle$ is slightly smaller in the As-rich side region (Fig. 3). The larger bowing of the two famatinite structures relative to the chalcopyrite structure is due to symmetry-allowed coupling between the X -derived and Γ -derived $\bar{\Gamma}$ state (Table II).

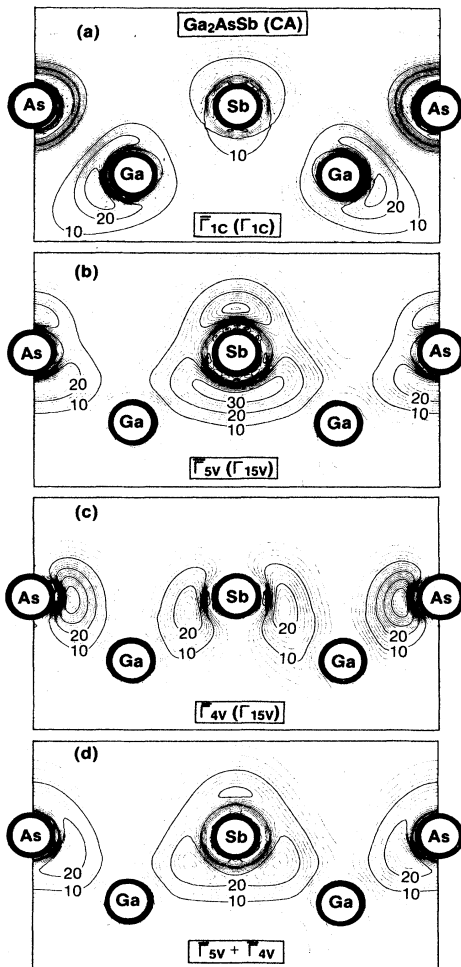


FIG. 9. Electronic charge-density contour plot of Ga_2AsSb in CuAu-I-like structure (in units of $10^{-3} e/\text{a.u.}^3$) for (a) the $\bar{\Gamma}_{1c}$ (Γ_{1c}) state, (b) the $\bar{\Gamma}_{5v}$ (Γ_{15v}) state, (c) the $\bar{\Gamma}_{4v}$ (Γ_{15v}) state, and (d) the weighted sum of (b) and (c).

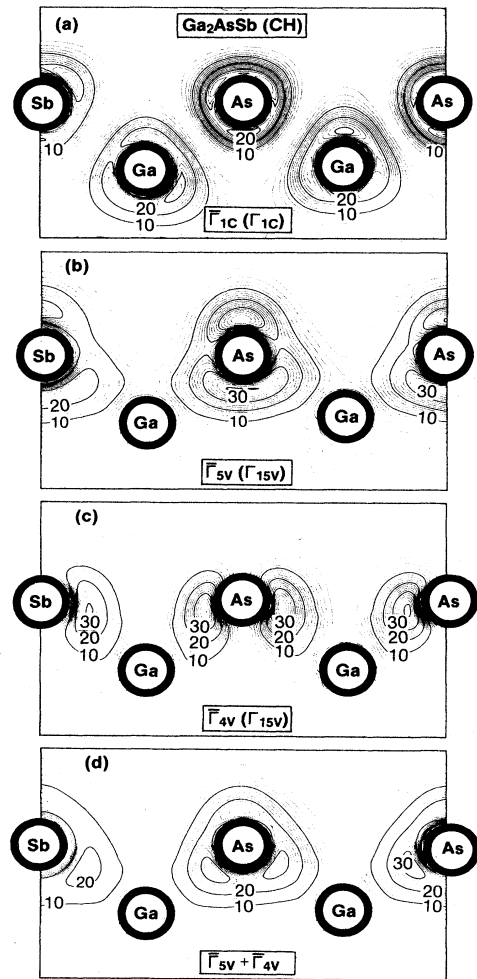


FIG. 10. Electronic charge-density contour plot of Ga_2AsSb in chalcopyrite structure (in units of $10^{-3} e/\text{a.u.}^3$) for (a) the $\bar{\Gamma}_{1c}$ (Γ_{1c}) state, (b) the $\bar{\Gamma}_{5v}$ (Γ_{15v}) state, (c) the $\bar{\Gamma}_{4v}$ (Γ_{15v}) state, and (d) the weighted sum of (b) and (c).

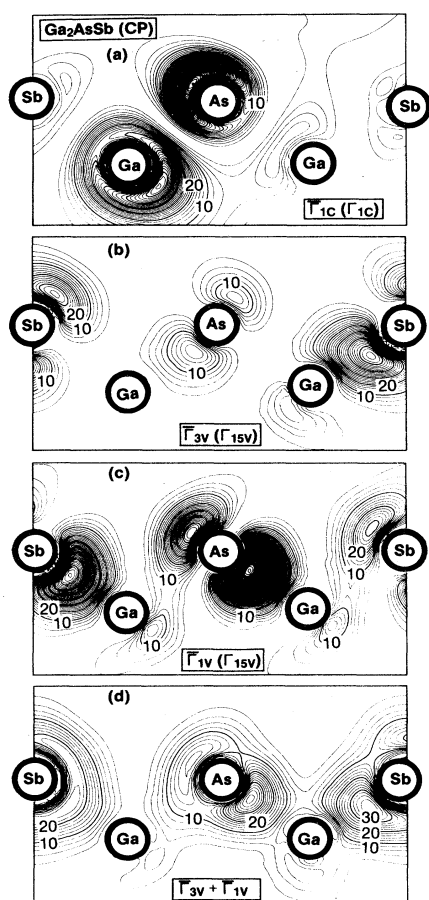


FIG. 11. Electronic charge-density contour plot of Ga_2AsSb in CuPt-like structure (in units of $10^{-3} e/\text{a.u.}^3$) for (a) the $\bar{\Gamma}_{1c}$ (Γ_{1c}) state, (b) the $\bar{\Gamma}_{3v}$ (Γ_{15v}) state, (c) the $\bar{\Gamma}_{1v}$ (Γ_{15v}) state, and (d) the weighted sum of (b) and (c).

Since GaAs, GaSb, and their alloys are direct-gap materials (cf. Fig. 3), folding of X states in the ordered ternary compounds does not change this basic situation. This is not the case in AlAs-GaAs alloys, as discussed next.

E. Ordered GaAs-AlAs compounds

Figure 12 depicts the LDA-corrected energy levels at $\bar{\Gamma}$ for GaAlAs_2 in the CuAu-I-like [Fig. 12(a)], chalcopyrite [Fig. 12(b)], and CuPt-like [Fig. 12(c)] structures, along with the energy levels of the binary constituents from which folding occurs. Table XV gives the angular-momentum decomposition of the wave functions at $\bar{\Gamma}$.

We find for this system that the VBM shows only negligible level repulsion and localization effects since Ga and Al have very similar p -orbital energies (Table IV). Therefore, the optical bowing for this system is almost entirely due to the bowing of the conduction states.

1. CuAu-I

The $\bar{\Gamma}_{1c}$ (Γ_{1c}) state is repelled downward by $\bar{\Gamma}_{1c}$ (X_{3c}) by 0.152 eV. The bowing coefficient for this transition is, therefore, $4 \times 0.152 = 0.61$ eV. Since Ga has a more tightly bound s orbital than Al (Table IV), the $\bar{\Gamma}_{1c}$ (Γ_{1c}) state tends to localize on the GaAs sublattice. The $\bar{\Gamma}_{4c}$ (X_{1c}) state is repelled upward by $\bar{\Gamma}_{4v}$ ($\bar{\Gamma}_{15v}$) by 0.07 eV but is still lower in energy than the $\bar{\Gamma}_{1c}$ (Γ_{1c}) state. Study of the energy levels away from the Brillouin-zone center show the conduction-band minimum for this system at \bar{R}_{1c} (L_{1c}) (at $\epsilon_v + 1.92$ eV) is due to "level segregation effects."²⁵ The next-highest state is \bar{M}_{5c} (X_{1c}) at 2.13 eV, followed by $\bar{\Gamma}_{4c}$ (X_{1c}) at 2.17 eV and $\bar{\Gamma}_{1c}$ (Γ_{1c}) at 2.18 eV. Hence, while the 50%-50% alloy is indirect at \bar{X}_{1c} (at 2.10 eV), the CuAu-I is indirect at \bar{R}_{1c} (L_{1c}). A detailed analysis of the electronic structure of GaAlAs_2 in the CuAu-I structure is given in Ref. 25.

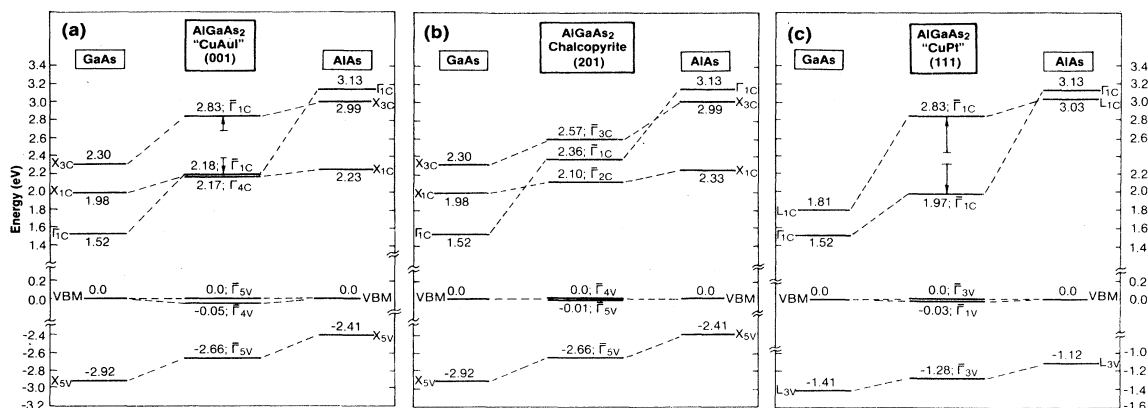


FIG. 12. LDA-corrected energy levels at $\bar{\Gamma}$ of AlGaAs_2 in the (a) CuAu-I-like, (b) chalcopyrite, and (c) CuPt-like structures. Dashed lines connect the folding states. Arrows depict the magnitude of the repulsion relative to the well centers.

TABLE XV. Calculated *l*-decomposed electron charges (in percent) inside the muffin-tin (MT) spheres of AlAs, GaAs, AlGaAs₂ (CH), and AlGaAs₂ (CP) at the zone center near the band edge. All the states are normalized to $2e/4$ -atoms cell. Electrons not included inside the MT spheres are in the interstitial regions. We use the MT-sphere radius $R_{\text{MT}} = 2.265$ a.u. for all atoms.

[illegible]

2. Chalcopyrite

As is the case for all other isovalent ternary compounds in the chalcopyrite structure, the energy levels of AlGaAs₂ in this structure [Fig. 12(b)] show much smaller optical bowing. The bowing for the $\bar{\Gamma}_{5v}(\Gamma_{15v})-\bar{\Gamma}_{1c}(\Gamma_{1c})$ transition is even slightly negative (-0.09 eV). The $\bar{\Gamma}_{5v}(\Gamma_{15v})$ state is below the $\bar{\Gamma}_{4v}(\Gamma_{15v})$ state by 0.01 eV, and, hence, like the chalcopyrite Ga₂AsSb [Fig. 6(b)], this system too has an “inverted” level arrangement.

3. CuPt

The energy levels are given in Fig. 12(c). Figure 4 shows that $\langle L_{1c} \rangle$ is very close in energy to $\langle \Gamma_{1c} \rangle$. Since both these states fold into $\bar{\Gamma}_1$ in the CuPt-like structure, this leads to a $\{\bar{\Gamma}_{1c}(\Gamma_{1c}); \bar{\Gamma}_{1c}(L_{1c})\}$ level repulsion of ± 0.36 eV (compared with ± 0.60 eV in Ga₂AsSb), and, hence, a $\bar{\Gamma}_{3v} \rightarrow \bar{\Gamma}_{1c}$ bowing coefficient of 1.45 eV. Despite the larger $\langle \Gamma_{1c} \rangle - \langle L_{1c} \rangle$ energy difference in GaAs-GaSb (Fig. 3), relative to to GaAs-AlAs (Fig. 4), the former systems show a greater level repulsion. This illustrates the role of structural relaxation (present only in GaAs-GaSb), which enhances the ordering potential of Eq. (1) and the fact that in common-cation systems repulsion of the VBM also contributes to the bowing.

The $\{\bar{\Gamma}_{1c}(\Gamma_{1c}); \bar{\Gamma}_{1c}(L_{1c})\}$ repulsion in CuPt-like GaAlAs₂ is found to be strong enough to offset the initial indirect gap of the disordered Ga_{0.5}Al_{0.5}As alloy (or the ordered CuAu-I-like system): we find for the ordered CuPt-like structure a *direct-gap* $\bar{\Gamma}_{1c}(\Gamma_{1c})$ gap at 1.97 eV, followed by the indirect *X*- and *L*-folded states at 2.03 and 2.13 eV.⁹⁴ This is a dramatic illustration of level-repulsion effects, converting an indirect-gap to a direct-gap material at the same composition. Yamaguchi⁹⁵ has calculated electronic structures of (GaAs)_n(AlAs)_n (111) superlattice for $n \geq 3$ using tight-binding method. As noted here, he found that unlike the (001) and (110) superlattices, the (111) superlattice is a direct-band-gap material even for an $n=3$ superlattice.

4. General trend for bowing in ordered GaAs-AlAs compounds

We find for Al_nGa_{4-n}As₄ that the bowing coefficients $b^{(a)}(X_n)$ are not only structure dependent, but that they also depend strongly on the concentration X_n (Table XIII). The reason for this abnormal behavior is that GaAs is a direct-gap material (Γ_{1c} lower in energy than X_{3c} and L_{1c}), whereas AlAs is an indirect-gap material (with Γ_{1c} above X_{3c} and L_{1c}). In this case, the relevant energy denominators of Eq. (1) depend strongly on composition (Fig. 4), leading to larger bowing for AlAs-rich compounds due to the near degeneracy of $\bar{\Gamma}_{1c}(\Gamma_{1c})$ and $\bar{\Gamma}_{1c}(X_{3c})$.

F. Analysis of volume deformation, chemical electronegativity, and structural relaxation effects on the direct gap of ordered ternary compounds

Table XVI gives the breakdown of the bowing parameter of the direct $\bar{\Gamma}_v \rightarrow \bar{\Gamma}_{1c}$ transition in the ordered ternary compounds into volume deformation (b_{VD}), chemical (b_{CE}), and structural relaxation (b_S) contributions, according to Eqs. (8)–(11). For comparison we give also previous results²² for the II-VI alloys, as well as results for GaInP₂ calculated here. These results suggest the following conclusions.

(i) The volume-deformation term b_{VD} is negligible for systems with a small lattice mismatch (GaAs-AlAs) or for systems with similar Γ_{1c} deformation potentials dE/da for the binary constituents (GaAs-GaSb, ZnS-ZnSe). This term is common to different crystal structures of the same composition since the equilibrium volumes depend only weakly on structures (Table IX).

(ii) The chemical-electronegativity term b_{CE} reflects the level repulsion [Eq. (1)] facilitated by the component of $\Delta V(r)$ due to chemical differences between the alloyed elements *A* and *B*. This term shows variations with crystal structure (as discussed in Sec. II B), reflecting the different degrees of coupling between folded-in states of different structures. For example, the chalcopyrite struc-

TABLE XVI. Contribution of volume deformation [VD, Eq. (8)], chemical electronegativity [CE, Eq. (9)], and structural relaxation [S, Eq. (10)] to the total (b_{tot}) bowing coefficient [Eq. (11)] of the direct $\Gamma_{15v}-\Gamma_{1c}$ -derived band gap in 50%-50% ordered semiconductor. The values for the Zn chalcogenides are taken from Ref. 22. All values in eV.

Compound	Structure	b_{VD}	b_{CE}	b_S	b_{tot}
Ga ₂ AsSb	CuAuI	-0.02	0.31	0.94	1.23
Ga ₂ AsSb	chalcopyrite	-0.02	-0.03	0.22	0.17
Ga ₂ AsSb	CuPt	-0.02	1.60	1.60	3.18
Zn ₂ SSe	CuAuI	-0.10	0.03	0.45	0.39
Zn ₂ SeTe	CuAuI	-0.36	1.00	1.32	1.96
Zn ₂ STe	CuAuI	-0.54	1.68	2.68	3.38
GaInP ₂	CuAuI	0.66	0.19	0.23	1.08
GaInP ₂	chalcopyrite	0.66	-0.13	-0.14	0.39
GaInP ₂	CuPt	0.66	0.82	0.34	1.82
GaAlAs ₂	CuAuI	0.0	0.61	0.0	0.61
GaAlAs ₂	chalcopyrite	0.0	-0.09	0.0	-0.09
GaAlAs ₂	CuPt	0.0	1.45	0.0	1.45

ture, having the weakest level-repulsion effects, also has the smallest b_{CE} . Since b_{CE} for a given structure reflects the chemical disparity between the alloyed elements, not surprisingly it scales with the $\chi_A - \chi_B$ electronegativity difference. Using the CuAu-I structure, we have b_{CE} values of 1.68, 1.0, 0.61, 0.31, 0.19, and 0.03 eV for the alloyed pairs S-Te, Se-Te, Ga-Al, As-Sb, Ga-In, and S-Se, respectively, whose Pauling^{96(a)} electronegativity differences—0.48, 0.45, 0.20, 0.13, 0.03, and 0.03, respectively—descend in the same order.

(iii) Structural bond relaxation (b_S) tends to dominate the bowing parameter in systems with a size mismatch. It reflects the level repulsion [Eq. (1)] facilitated by the component of $\Delta V(r)$ due to the size difference in the alloyed elements A and B . Not surprisingly, it scales with the size mismatch $\Delta R = R_A - R_B$, showing for the common-cation CuAu-I structure b_S values of 2.68, 1.32, 0.94, and 0.45 eV for the alloyed pairs S-Te, Se-Te, As-Sb, and S-Se, respectively, having the differences 0.28, 0.18, 0.18, and 0.10 Å, respectively, in the Pauling tetrahedral radii.^{96(b)} While b_{VD} reflects hydrostatic deformation potentials, b_S reflects frozen-phonon deformation potentials associated with the particular lattice distortions of Table XI.

Our results, as well as those of Bernard and Zunger²² and Zunger and Jaffe,²⁴ show that the distortion of the common sublattice C in $A_x B_{1-x} C$ has a very important role in the optical bowing of the direct band gap, an effect neglected in all virtual-crystal-approximation (VCA) calculations on bowing.^{52–56}

G. Comparison of predicted ordering-induced changes in the band gaps with experiment

Despite a recent surge in observations of ordering in isovalent semiconductor alloys,^{28–36} very few optical experiments have been conducted so far on these novel structures. Most of our predictions await, therefore, experimental testing.

A number of experiments^{38,39} were recently conducted on the CuAu-I form of GaAlAs₂ (i.e., an alternate monolayer superlattice in the [001] direction). Ellipsometry measurements³⁸ of the $E_0(\bar{\Gamma}_v \rightarrow \bar{\Gamma}_{1c})$ transition give a transition energy of 2.08 eV at room temperature, or ~ 2.18 eV when extrapolated to low temperature, in agreement with our calculated value (2.18 eV, Table X). Low-temperature Raman experiments³⁹ similarly show a strong resonance at 2.15 eV, which we associate with the same transition. These results are interesting in the sense that they demonstrate a downward shift of the $\bar{\Gamma}_{15} \rightarrow \bar{\Gamma}_{1c}$ gap relative to the disordered alloy [$\sim 2.20 \pm 0.02$ eV (Ref. 97) at low temperature]. The pseudodirect $\bar{\Gamma}_{1c}$ (X_{3c}) state predicted to occur at 2.83 eV (Table XII) was not seen yet, presumably because it is weak and overlaps with other direct transitions.

The lowest conduction band in the CuAu-I form of GaAlAs₂ is predicted to be $\bar{R}_1(L_{1c})$ at 1.92 eV. Garriga *et al.*³⁹ and Isu *et al.*⁹⁸ observed a single-line low-temperature photoluminescence with no resolved phonon side bands at 1.931 eV, which we identify with emission from $\bar{R}_1(L_{1c})$. An earlier study by Ishibashi *et al.*⁹⁹ found this photoluminescence at 2.05 eV, presumably due

to partial disorder in his sample (the disordered alloy of the same composition has an emission at ¹⁰⁰ ~ 2.08 eV).

Similar evidence for the reduction of the E_0 gap upon ordering was found by Fukui and Saito,²⁸ who grew GaInAs₂ in the CuAu-I structure, finding at 77 K a photoluminescence peak at 0.765 eV, i.e., 35 meV lower than the value (0.800 eV) of the disordered alloy of the same composition.

Experimental information on the optical properties of CuPt-like ordered semiconductors is far more fragmentary. Gomyo *et al.*^{33(a)} found CuPt-like ordered domains in GaInP₂ exhibiting in photoluminescence a room-temperature direct gap of 1.85 eV, lower than the value of 1.912 eV she finds for the disordered alloy of the same composition. While the precise value of the gap depended on the extent to which the growth conditions (III/V ratio, growth rate, and temperature) facilitated ordering, a clear reduction in the gap upon ordering was seen in all samples. This 60-meV reduction at $E_g \sim 1.9$ eV corresponds to a shift of about 200 Å in photon wavelength of a GaInP₂ laser. A similar shift was seen by Kurtz *et al.*^{33(b)} in electroreflectance measurements. Taking for the $\Gamma_{15} \rightarrow \Gamma_{1c}$ transition energies in GaP and InP the room-temperature values of 2.78 and 1.34 eV, respectively⁶⁹ (average: 2.06 eV), and Gomyo's value of 1.85 eV for the partially ordered sample, we find an experimental bowing parameter of $4(2.06 - 1.85) = 0.84$ eV for the ordered GaInP₂, far smaller than the value of 1.82 eV obtained here (Table XVI) for perfect CuPt ordering. We have no explanation for this difference except the hypothesis that the GaInP₂ sample³³ may be only partially ordered or may contain also domains of different types of ordering (chalcopyrite, CuAu-I) with smaller bowing coefficients (Table XVI) as well as antiphase boundaries, which may dominate the band-gap value. The same explanation seems pertinent to the observed modest decrease in the band gap of Ga₂AsSb upon ordering³² (≤ 0.1 eV), compared with the larger decrease predicted for the perfectly ordered case (Table XIII). In another electroreflectance study on GaInP₂, Nishino *et al.*¹⁰¹ have also observed a new 1.7-eV structure (for samples grown at 600°C), which they ascribe to a possible defect. According to our calculation, this might be the transition to $\bar{\Gamma}_{1c}(\Gamma_{1c})$ which we find at ~ 1.6 eV.

H. Bowing of the spin-orbit splitting Δ_0 in ordered structures

For the $Al_n Ga_{4-n} As_4$ system we find $\Delta_0(\text{GaAs}) \simeq 0.338$ eV, $\Delta_0(\text{AlAs}) = 0.303$ eV, and a spin-orbit bowing parameter $b_n(\Delta_0) \simeq 0$ for all the ternary $Al_n Ga_{4-n} As_4$ compounds. These results are consistent with the very small repulsion and localization of the valence states in this system (Sec. VD). The situation is quite different in $Ga_4 As_n Sb_{4-n}$, where repulsion effects exist also in the valence band. There we find that all the bowing coefficients¹⁰² $b_n(\Delta_0)$ of $Ga_4 As_n Sb_{4-n}$ (Table XIII) are negative [i.e., $\Delta_0(X_n)$ is upward concave]. The magnitude of $b_n(\Delta_0)$ is large when $b_n(E_g)$ is large, e.g., Table XIII.

The increase of Δ_0 in the ternary structures reflect the higher localization of the wave function on the Sb site relative to the binary constituents (Figs. 7–11). In Table XIV we show the angular-momentum-decomposed

charge within the muffin-tin spheres of the VBM and CBM states at $\bar{\Gamma}$ for Ga_2AsSb in the chalcopyrite, CuAu-I , and CuPt structures and for their binary constituents. The results of Table XIV indicate that repulsion-induced localization is caused primarily by *intraband* repulsion since the angular-momentum character of the VBM states (pure p states in binaries) is essentially unchanged. Interband repulsion, which mixes the s and p character at $\bar{\Gamma}$, is rather weak ($<2\%$ inside the MT spheres) and, therefore, has little effect on Δ_0 for the ordered ternary compound. Since the VBM of GaSb is higher in energy than the VBM of GaAs (Fig. 5), the VBM charge in Ga_2AsSb is preferentially localized on the Sb sublattice. Furthermore, since the lattice constant of Ga_2AsSb is smaller (larger) than that of GaSb (GaAs), this leads to a larger (smaller) volume renormalization of the atomic spin-orbit splitting for Sb (As). Since $\Delta_0(\text{GaSb})$ is larger than $\Delta_0(\text{GaAs})$ (Table VI), renormalization and repulsion-induced localization cause the negative bowing coefficient found in our calculation of $\text{Ga}_4\text{As}_n\text{Sb}_{4-n}$ system. We expect this to be a general trend since in all common-cation ordered compounds the binary component with heavier anion (e.g., Sb) usually has a higher VBM and a larger lattice constant than the component with a lighter anion (e.g., As). Consequently, the VBM of ordered ternary compounds are expected to be more localized on the heavier anion sublattice than is the case in the binary constituents. This will enhance Δ_0 in the ternary phase, hence producing a negative bowing for the spin-orbit splitting Δ_0 at $\bar{\Gamma}$. For common anion systems b (Δ_0) is generally small since Δ_0 depends weakly on cations.

VI. RESULTS FOR DISORDERED TERNARY ALLOYS

A. Bowing of the direct band gap in the disordered alloy

The composition variation of the band gap $\varepsilon_g(x)$ of disordered alloys has been customarily described as^{2,3,50,51}

$$\varepsilon_g(x) = \bar{\varepsilon}_g(x) - bx(1-x), \quad (12)$$

where $\varepsilon_g(x)$ is the band gap of the disordered alloy and $\bar{\varepsilon}_g(x) = x\varepsilon_{AC} + (1-x)\varepsilon_{BC}$ is the concentration-weighted average gap. Still a very popular approach for calculating b rests on the virtual-crystal approximation⁵²⁻⁵⁶ (VCA), in which the individual A and B sublattices are replaced by an average ("virtual") $\langle AB \rangle$ sublattice, characterized by an average potential $\langle V \rangle = xV_A$

$+ (1-x)V_B$. Since band energies are generally nonlinear functions of the potential,^{52,103} this potential-averaging technique is guaranteed to produce a nonzero bowing. It has been recently shown,²² however, that by using empirical band-structure techniques it is possible to obtain almost any value of b (by parameter adjustment) without affecting the overall quality of the fit¹⁰⁴ of the band energies of the binary constituents to experiment. When nonempirical band-structure methods are used,^{21,27} the VCA tends to underestimate the bowing considerably. To account for such discrepancies, one often proceeds to theories such as the sites-only coherent-potential approximation^{26,61} (denoted CPA), or its molecular version.²⁷ Although improved results are found, the discrepancy between theory and experiment is still sizable, especially for systems with large bowing parameters.²⁷

Our own point of view (Refs. 21-25) is that for most of the alloys, the ordering potential $\Delta V(\mathbf{r})$ is too strong to be neglected (VCA) or treated by a low-order (site-only) CPA. We believe that, like in ordered compound, in disordered alloy the ordering potential resulting from the structural dissimilarities (reflected in differences in the average $A-C$ and $B-C$ bond lengths) as well as the chemical dissimilarities will lead to level repulsion, and, hence, bowing. This level-repulsion effect is neglected altogether in VCA and is treated to lowest order in the molecular CPA.

A sensible theory of optical bowing in disordered alloys could hence be based on finding a special configuration of A and B atoms on a lattice which best represents, in a statistical sense, the true ensemble average of the alloy as sampled by electronic wave functions. Applying periodic boundary conditions to this atomic configuration and using band-theoretic techniques to find its electronic structure could hence establish the spectrum of this "representative alloy." Unfortunately, such a representative unit cell, small enough to be conducive to band calculations, has not been found yet.

Zunger and Jaffe²⁴ suggested that the chalcopyrite structure may serve as a crude approximation to this "representative alloy." Our present calculation and that of Ref. 89 (all LAPW) (see also Figs. 13 and 14 below), as well as those of Bernard and Zunger²² (on the Zn chalcogenides, using mixed basis) show that the CuAu-I unit cell works even better: the calculated bowing parameters at $x=0.5$ for the fundamental direct gap of this ordered structure form a reasonable first approximation to the measured alloy bowing:

$$\begin{aligned} \text{ZnSSe: } b_{\text{calc}} &= 0.39 \text{ and } b_{\text{expt}} = 0.43 \text{ (Ref. 105) ,} \\ \text{ZnSeTe: } b_{\text{calc}} &= 1.96 \text{ and } b_{\text{expt}} = 1.23 \text{ (Ref. 106) ,} \\ \text{ZnSTe: } b_{\text{calc}} &= 3.83 \text{ and } b_{\text{expt}} \cong 3 \text{ (Ref. 107) ,} \\ \text{GaAsSb: } b_{\text{calc}} &= 1.23; \text{ and } b_{\text{expt}} = 1.0-1.2 \text{ (Ref. 108) ,} \\ \text{GaAlAs: } b_{\text{calc}} &= 0.61 \text{ and } b_{\text{expt}} = 0.37 \text{ and } 0.68 \text{ (Refs. 109 and 110) ,} \\ \text{CdHgTe: } b_{\text{calc}} &= 0.05 \text{ and } b_{\text{expt}} = 0.0 \text{ and } 0.23 \text{ (Ref. 89) ,} \\ \text{HgZnTe: } b_{\text{calc}} &= 0.41 \text{ and } b_{\text{expt}} = 0.14 \text{ (Ref. 89) ,} \\ \text{CdZnTe: } b_{\text{calc}} &= 0.44 \text{ and } b_{\text{expt}} = 0.26 \text{ (Ref. 89) .} \end{aligned} \quad (13)$$

Clearly, the ordered CuAu-I structure forms a much better zero-order choice for perturbation theory than does the virtual crystal. The CuAuI structure is also a better “representative alloy” than the chalcopyrite structure, since it captures the VD, CE, and S contributions to the bowing (Table XVI), whereas the chalcopyrite structure captures mainly the VD contribution.

A further attempt to improve the results is based on adding to the CuAu-I contribution (representing an A_2B_2 local environment around the common C atom) the other four possible local environments, e.g., the A_4 cluster (modeled by the zinc-blende AC crystal), the A_3B cluster (luzonite A_3BC_4), the AB_3 cluster (luzonite AB_3C_4), and the B_4 cluster (zinc-blende BC). Denoting by $P_n(x)$ the probability of finding cluster n (of $A_nB_{4-n}C_4$) at the composition x , and by $a(x)$ the alloy lattice parameter at x , the average band gap can be modeled²² as

$$\epsilon_g(x) = \sum_{n=0}^4 P_n(x) \epsilon_g^{(n)}[a(x)] . \quad (14)$$

Band-structure calculations for the five (0,0,1) ordered structures $A_nB_{4-n}C_4$ at a given $a(x)$ value give $\{\epsilon_g^{(n)}[a(x)]\}$, and hence, $\epsilon_g(x)$ of Eq. (14) at this composition. Using Eq. (12) one then finds b at this x value. Posternak *et al.*¹¹¹ have simplified Eq. (14), approximating $\epsilon_g(x = X_n) = \epsilon_g^{(n)}(a_{eq}^{(n)})$, i.e., equating the band gap of the disordered alloy at $x = \frac{1}{4}, \frac{1}{2}$, and $\frac{3}{4}$ with the band gaps of $AlGa_3As_4$, $AlGaAs_2$, and Al_3GaAs_4 , respectively.

We applied the superposition model of Eq. (14) to calculate the bowing in $GaAs_{1-x}Sb_x$ and $Al_xGa_{1-x}As$, using for $P_n(x)$ and random tetrahedral probability.

1. $GaAs_xSb_{1-x}$

To find $\epsilon_g^{(n)}[a(x)]$ used in Eq. (14), we have assumed

$$\epsilon_g^{(n)}[a(x)] = \epsilon_g^{(n)}(a_n) + \frac{d\epsilon_g^{(n)}}{da} [a(x) - a_n] , \quad (15)$$

where a_n and $\epsilon_g^{(n)}(a_n)$ are the calculated equilibrium lattice constant (Table IX) and band gap at a_n (Table X), respectively. We have approximated $a(x)$ using Vegard's rule and have let

$$\frac{d\epsilon_g^{(n)}}{da} = X_n \frac{d\epsilon_g^{AC}}{da} + (1 - X_n) \frac{d\epsilon_g^{BC}}{da} , \quad (16)$$

where $d\epsilon_g^{AC}/da = -3.51$ eV/Å and $d\epsilon_g^{BC}/da = -3.95$ eV/Å are the deformation potential for GaSb and GaAs, respectively, calculated at their respective equilibrium position. Using Eqs. (14)–(16) we find for the direct transition in disordered $GaAs_{1-x}Sb_x$ (in eV)

$$b(x) \approx 0.86 \quad (17)$$

(b is slightly larger on the As-rich side). We find from direct calculation that the assumption of linearity [Eqs. (15) and (16)] underestimates $b(x)$ of Eq. (14) at $x=0.5$ by about 0.06 eV. The calculated composition variation of the direct band gap (before and after application of the LDA correction) is plotted in Fig. 13, together with the

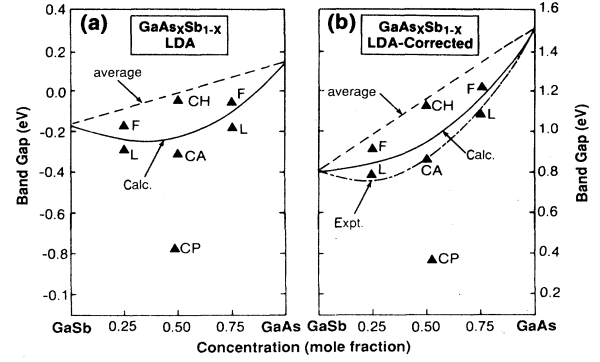


FIG. 13. Calculated concentration variation of the energy gap $E_g(\Gamma_{1c} - \Gamma_{15v})$ of the $GaAs_xSb_{1-x}$ alloy (solid line). Dashed lines give the linear concentration-averaged band gap; band gaps of the ordered ternary compound are shown as solid triangles. Using (a) the LDA and (b) LDA-corrected results (see text). The experimental values (Ref. 108) (dotted-dashed line) with $b = 1.2$ eV is also given in (b) for comparison.

calculated band gap of ordered structures. The calculated bowing parameter is somewhat smaller than experimental values $b \approx 1.0 - 1.2$ eV.¹⁰⁸ However, in the calculation we have assumed random probability. If clustering occurs (as predicted in our phase-diagram calculation³⁷) b will increase, because mixing of end-point clusters A_4C and B_4C reduces the bowing coefficient of $GaAs_{1-x}Sb_x$ since b_{VD} is very small for this system (Table XVI).

2. $Al_xGa_{1-x}As$

We find for the direct transition $\Gamma_{15v} \rightarrow \Gamma_{1c}$ in this system

$$b(x) = 0.58 + 1.06(x - 0.5) , \quad (18)$$

which is strongly concentration dependent. Since most experiments were done in the region $x < 0.4$ (where the system is direct), the small optical bowing observed¹⁰⁹ for this composition range (0–0.37 eV) is consistent with our calculation. Anticlustering predicted for this system³⁷ will further reduce $b(x)$.

While for most semiconductor alloys Eq. (12) provides an adequate fit to the data, our results above show that $Al_xGa_{1-x}As$ is an exception. The dependence of b on composition can be traced to the fact that AlAs is an indirect-gap material: Since the level repulsion $[\delta E$ of Eq. (1)] depends inversely on the energy denominator $\Delta\epsilon$, and since the latter is strongly composition dependent for the $\langle \Gamma_{1c} \rangle - \langle X_{3c} \rangle$ pair (exhibiting even a crossing, see Fig. 4), we find a considerably smaller b in the Ga-rich composition range than in the Al-rich range. Such a composition dependence of $b(\Gamma_{15v} \rightarrow \Gamma_{1c})$ gap was noted by Dingle *et al.*¹¹⁰ and by Monemar *et al.*,¹¹² who find $b = \alpha + \beta x$ with $\beta = 1 - 1.15$ eV. Monemar *et al.*¹¹² excluded the possibility that this anomaly is due to Γ - X coupling based on the fact that for $x > \sim 0.4$, the X_{1c} state is lower in energy than the Γ_{1c} state, and, hence, coupling between Γ_{1c} and X_{1c} will increase the Γ_{1c} gap; our symmetry analysis shows, however, that their

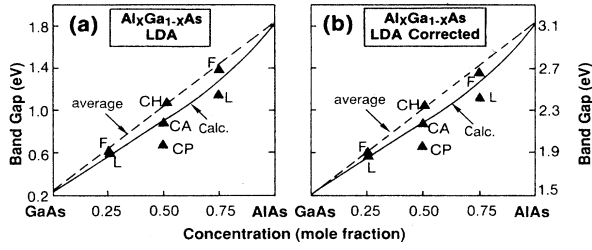


FIG. 14. Calculated concentration variation of the energy gap $E_g(\Gamma_{1c}-\Gamma_{15v})$ of the $\text{Al}_x\text{Ga}_{1-x}\text{As}$ alloy (solid line). Dashed lines give the linear concentration-averaged band gap; band gaps of the ordered ternary compound are shown as solid triangles. Using (a) the LDA and (b) LDA-corrected results (see text).

analysis is incorrect since it is the $X_{3c}-\Gamma_{1c}$ coupling which is responsible for the anomalous composition dependence of $\bar{\Gamma}_{1c}$.

Our calculated results demonstrate that the model of Eq. (14) can adequately reproduce the experimentally observed band-gap variations, suggesting that in the disordered alloy level repulsion is an important mechanism of the optical bowing. Even though the success of the superposition model in calculating $b(x)$ is encouraging and can be rationalized by noticing that some effects neglected in the model cancel each other, further study is required to see why the superposition of (0,0,1) ordering vector structures (zinc-blende, lúzonite, and CuAu-I) appear to represent reasonably well the $\Gamma_v-\Gamma_{1c}$ optical transition of the “average alloy.”

B. Bowing of the spin-orbit splitting Δ_0 in disordered alloys

In analogy with Eq. (12), the composition variation of the Δ_0 spin-orbit splitting has been fitted to the form

$$\Delta_0(x) = \bar{\Delta}_0(x) - b(\Delta_0)x(1-x), \quad (19)$$

where $b(\Delta_0)$ is the bowing parameter. For all ordered GaAs-GaSb structures we find (Table XIII) $b(\Delta_0) < 0$. For the disordered alloy $b(\Delta_0)$ of Eq. (19) is -0.08 eV. The experimental situation pertaining to the magnitudes of $b(\Delta_0)$ can be summarized as follows.

(i) *Epitaxially* grown lattice-matched samples show $b(\Delta_0) < 0$, i.e., an *enhancement* of the spin-orbit splitting over the linear average value. This is the case for InGaAsP/InP, where $b(\Delta_0) \simeq -0.09$ eV (Refs. 113–117) and in GaAlInAs/InP, where $b(\Delta_0) \simeq -0.10$ eV.¹¹⁸

(ii) *Bulk* grown alloys are said^{119,120} to exhibit $b(\Delta_0) > 0$, whereas our calculation for GaAsSb shows $b(\Delta_0) < 0$. The experimental situation here deserves further discussion.

Most of the experimental studies on $b(\Delta_0)$ in bulk III-V alloys were carried out in the 1960s by Woolley and co-workers.^{50,60,119,120} In any early study,¹¹⁹ Berolo and Woolley found that numerous III-V systems show positive $b(\Delta_0)$ values, in excess of ~ 0.1 eV (a typical uncertainty in the data), e.g.,¹¹⁹ 0.175 eV for GaAsP, 0.357 eV for InAsP, 1.17 eV for InAsSb, 0.101 eV for GaInP, and 0.144 eV for GaInAs. Latter on,¹²⁰ these authors have

revised two of these values to lower numbers, e.g., 0.02 ± 0.04 eV for GaAsP and 0.08 eV for InAsP. Negative bowings were, however, found for GaInP, $b(\Delta_0) = -0.05$ eV (Ref. 121) and for GaAsP, $b(\Delta_0) \simeq -0.03$ eV.⁶⁰ InAsSb has yielded the largest $b(\Delta_0)$ value of all systems. Unfortunately, no spectra were given. However, since this system shows only limited solid solubility,¹²² the bulk samples obtained showed a very large composition gradient and the optical spectra were, hence, seen clearly⁵⁰ only for samples with less than 15% InAs. The value $b(\Delta_0) = 0.144$ eV given in Refs. 119 and 120 for GaInAs is said to have been measured in Ref. 123. This paper reports room-temperature infrared-absorption data (Fig. 2 of Ref. 123) which disagree with previous data reported in Ref. 123; no resolved spin-orbit splitting is seen in either data.

We conclude that there is no strong evidence for $b(\Delta_0) \gg 0$ in III-V alloys. In II-VI alloys, $b(\Delta_0) < 0$ was observed, e.g., in ZnSeTe (Ref. 124), $b(\Delta_0) = -0.59$ eV.

The theoretical situation pertaining to $b(\Delta_0)$ in III-V alloys is no less confusing than the experimental situation. Most authors^{51,120,125,126} tried to account for $b(\Delta_0) > 0$. Woolley and his collaborators observed empirically that there is an approximate linear scaling between $b(\Delta_0)$ and the bowing $b(E_0)$ of the direct band gap. Van Vechten *et al.*¹²⁰ have, therefore, advanced a scaling argument to the effect that

$$b(\Delta_0) = \alpha b(E_0), \quad (20)$$

where

$$\alpha = \frac{\bar{\Delta}_0(x)}{3} \left[\frac{2}{\bar{E}_0(x)} + \frac{1}{\bar{E}_0(x) + \bar{\Delta}_0(x)} \right]. \quad (21)$$

Here, $\bar{\Delta}_0(x)$ and $\bar{E}_0(x)$ are the linear averages of the Δ_0 and E_0 gaps of the end-point compounds. To rationalize Eqs. (20) and (21), Van Vechten *et al.* argued that $b(\Delta_0)$ is dominated by interband coupling. In their argument, it is assumed that the disorder present in these alloys will mix a fraction $Q_s(x)$ of the conduction-band s character into the top of the valence band, and, hence, displacing an equivalent amount of p character. This will, therefore, reduce Δ_0 by a factor $1 - Q_s$, or

$$\Delta_0(x) = \bar{\Delta}_0(x) - Q_s(x)\bar{\Delta}_0(x), \quad (22)$$

where $Q_s(x)$ is inversely proportional to the average band gap. Hill¹²⁵ pointed out that Eqs. (20) and (21) are merely scaling *assumptions*; postulating that $\alpha = \bar{\Delta}_0(x)/\bar{E}_0(x)$, he could explain the data¹¹⁹ even slightly better.

While the scaling rules of Eqs. (20) and (21) seem to work well, they do confront some difficulties: to explain experiments, this approach requires that as much as 50% of the conduction-band s character be mixed into the valence band,¹²⁰ whereas our first-principles calculations (Table XV) grant at most, $Q_s(0.5) = 3\%$. Furthermore, since s - p mixing repels the conduction band to *higher* energies, it leads to $b(E_0) < 0$, in conflict with the data.

Chadi¹²⁶ has proposed a perturbation treatment in which the disorder-induced potential fluctuation mixes s character into the valence band, thereby reducing Δ_0 .

Adjustment of the tight-binding matrix elements describing this perturbation led to a good fit of the experimental data. Ling and Miller¹²⁷ argued that this perturbation is too large for perturbation theory to be valid. They have calculated this mixing using a superposition approach, showing that it leads $b(\Delta_0)$ values which are considerably smaller than the experimentally reported values.

Our discussion above suggests that there is no rigorous quantitative theory currently available to describe the large nonlinear deviation of $\Delta_0(x)$ observed in experiment.¹¹⁹ Further study on this subject both experimentally and theoretically appears desirable. Since alloying may also split the heavy-hole and light-hole states at the VBM, crystal-field splitting should also be taken into account to interpret experimental data.

VII. SUMMARY

We have studied the electronic structures of ordered ternary compounds $\text{Ga}_4\text{As}_n\text{Sb}_{4-n}$ and $\text{Al}_n\text{Ga}_{4-n}\text{As}$ by performing first-principles band-structure calculations. We find that states at different \mathbf{k} point of zinc-blende Brillouin zone are coupled in ternary compounds by the non-zinc-blende ordering potential, leading to substantial level repulsion and sensitively determining the energy levels and charge redistributions in ternary compounds. We find the following.

(i) Level repulsion leads to a reduction of the fundamental band gap of the ternary compound relative to the linear average of its binary constituents.

(ii) This level repulsion depends on the crystal structure (determining which zinc-blende states are folded into the same symmetry) and on the energy denominator (i.e., level separation between these unperturbed zinc-blende states). In the (001) $n=1$ superlattice (the CuAu-I structure), the conduction-band energy shifts are ± 0.15 eV for $\{\bar{\Gamma}_{1c}(X_{3c}); \bar{\Gamma}_{1c}(\Gamma_{1c})\}$ in AlGaAs_2 and ± 0.24 eV for $\{\bar{\Gamma}_{1c}(X_{1c}); \bar{\Gamma}_{1c}(\Gamma_{1c})\}$ in Ga_2AsSb . In the (111) $n=1$ superlattice (the CuPt structure), the conduction-band level shifts are larger: ± 0.36 eV for $\{\bar{\Gamma}_{1c}(\Gamma_{1c}); \bar{\Gamma}_{1c}(L_{1c})\}$ in AlGaAs_2 and ± 0.60 eV for the same pair in Ga_2AsSb . These conduction-band level repulsions alter the wave functions, enhancing localization on the Ga-As sublattice in AlGaAs_2 and Ga_2AsSb ; they make the CuPt form of AlGaAs_2 a direct-gap material even though the 50%-50% alloy is indirect.

(iii) Level repulsion is generally smaller in the valence bands, e.g., ± 0.085 eV for the $\{\bar{\Gamma}_{5v}(X_{5v}); \bar{\Gamma}_{5v}(\Gamma_{15v})\}$ pair in CuAu-I-like Ga_2AsSb and ± 0.19 eV in the $\{\bar{\Gamma}_{3v}(L_{3v}); \bar{\Gamma}_{3v}(\Gamma_{15v})\}$ pair in CuPt-like Ga_2AsSb . These valence-band repulsion effects enhance the wave-function localization in the VBM states of Ga_2AsSb on the Sb sublattice. In the $n=2$ (201) superlattice (chalcopyrite structure), we find an *inverted* structure, whereby the $\bar{\Gamma}_{5v}$ state is below $\bar{\Gamma}_{4v}$. We predict that if one of the binary constituents is an indirect-gap material (e.g., AlAs, GaP, etc.), the bowing coefficient of Eq. (17) will be composition dependent. It will increase when the repelling states approach each other.

(iv) At $X_n = \frac{1}{2}$, we find $E_g^\Gamma(\text{CP}) < E_g^\Gamma(\text{CA}) < E_g^\Gamma(\text{CH})$.

(v) Bond-length mismatch between $A-C$ and $B-C$

increases the bowing—it is often the dominant factor for common-cation lattice-mismatched alloys.

(vi) Bowing coefficients of the spin-orbit splitting at the VBM for ordered common-cation ternary compounds are negative, due to repulsion-induced state localization, in contrast to the experimental observation that $b(\Delta_0)$ is always positive for disordered isovalent semiconductor alloys.

We have studied the relation between bowing in ordered structures and that in disordered alloys. We find, as a first-order approximation, that structure with a (001) ordering vector can be used as “representative alloy” to find the bowing coefficients for the $\Gamma_{15v}-\Gamma_{1c}$ transition. Results obtained from the superposition approach are in good agreement with experimental values. Previous descriptions of the bowing of the spin-orbit splitting at the VBM are not supported by our calculation. We believe that further study of $b(\Delta_0)$ experimentally as well as theoretically is needed, which should also take into account the crystal-field splitting at the VBM.

ACKNOWLEDGMENTS

We thank J. E. Bernard for useful discussions. This work was supported by the U.S. Department of Energy (DOE) under Grant No. DE-AC02-77CH00178.

APPENDIX: ORDER OF X_{1c} AND X_{3c} STATES IN ZINC-BLENDE SEMICONDUCTORS

Placing the origin of the coordinate system on the anion, minimal-basis-set tight-binding models^{59,80} give the following energies of the X_{1c} and X_{3c} conduction states:

$$\begin{aligned}\epsilon(X_{1c}) &= \frac{1}{2}(\epsilon_p^c + \epsilon_s^a) + \left[\frac{1}{4}(\epsilon_p^c - \epsilon_s^a)^2 + V_{sp}^2 \right]^{1/2}, \\ \epsilon(X_{3c}) &= \frac{1}{2}(\epsilon_p^a + \epsilon_s^c) + \left[\frac{1}{4}(\epsilon_p^a - \epsilon_s^c)^2 + V_{sp}^2 \right]^{1/2}.\end{aligned}\quad (\text{A1})$$

Here, c and a denote cation and anion, respectively, and V_{sp} is the coupling matrix element, scaling⁵⁹ as d^{-2} , where d is the anion-cation bond length. At the limit of large interatomic separation $V_{sp} \rightarrow 0$ and

$$\begin{aligned}\epsilon(X_{1c}) &= \epsilon_p^c, \\ \epsilon(X_{3c}) &= \max(\epsilon_p^a, \epsilon_s^c).\end{aligned}\quad (\text{A2})$$

Since $\epsilon^a < \epsilon^c$, this leads to $\epsilon(X_{1c}) > \epsilon(X_{3c})$. At the limit of short interatomic distances, where V_{sp}^2 overwhelms the difference in orbital energies, $\epsilon(X_{1c}) = \epsilon(X_{3c})$.

Since

$$\begin{aligned}\frac{\partial \epsilon(X_{1c})}{\partial d} &= \frac{-\frac{2}{d} V_{sp}^2}{\left[\frac{1}{4}(\epsilon_p^c - \epsilon_s^a)^2 + V_{sp}^2 \right]^{1/2}} < 0, \\ \frac{\partial \epsilon(X_{3c})}{\partial d} &= \frac{-\frac{2}{d} V_{sp}^2}{\left[\frac{1}{4}(\epsilon_p^a - \epsilon_s^c)^2 + V_{sp}^2 \right]^{1/2}} < 0,\end{aligned}\quad (\text{A3})$$

and since $|\epsilon_p^a - \epsilon_s^c| < |\epsilon_p^c - \epsilon_s^a|$, one has

$$\frac{\partial[\varepsilon(X_{1c}) - \varepsilon(X_{3c})]}{\partial d} > 0, \quad (\text{A4})$$

so that $\varepsilon(X_{1c}) - \varepsilon(X_{3c})$ is a monotonic function of d . Combined with the discussion surrounding Eq. (A2), this shows that

$$\varepsilon(X_{1c}) > \varepsilon(X_{3c}) \text{ for all } d > 0, \quad (\text{A5})$$

in obvious conflict with other calculations (e.g., Table VII).

Since the pressure derivative $d\varepsilon/dp$ has the opposite sign of $\partial\varepsilon/\partial d$, Eq. (A3) also shows that

$$d\varepsilon/dp > 0 \quad (\text{A6})$$

for both X_{1c} and X_{3c} , in conflict with experiment (Table VI).

Equations (A1) and our discussion provides, however, simple guidance for understanding the order of X_{1c} and X_{3c} states: for systems with sufficiently large lattice parameters (hence, sufficiently small V_{sp}), sufficiently shallow anion s states and sufficiently deep cation s states X_{3c} will be below X_{1c} . We find this to be the case for GaSb and HgTe.

- ¹J. C. Woolley, in *Compound Semiconductors*, edited by R. K. Willardson and H. L. Goering (Reinhold, New York, 1962), p. 3.
- ²D. Long, in *Semiconductors and Semimetals*, edited by R. K. Willardson and A. C. Beer (Academic, New York, 1966), Vol. 1, p. 143.
- ³O. Madelung, *Physics of III-V Compounds* (Wiley, New York, 1964), p. 269.
- ⁴H. C. Casey and M. B. Panish, *Heterostructure Lasers* (Academic, New York, 1978), Chap. 4.
- ⁵T. P. Pearsall, *GaInAsP Alloy Semiconductors* (Wiley, New York, 1982).
- ⁶M. Jaros, Rep. Prog. Phys. **48**, 1091 (1985).
- ⁷M. B. Panish and M. Ilegems, Prog. Solid State Chem. **7**, 39 (1972).
- ⁸G. B. Stringfellow, J. Cryst. Growth **27**, 21 (1974); J. Phys. Chem. Solids **23**, 665 (1972).
- ⁹J. Van Vechten, in *Handbook of Semiconductors*, edited by S. P. Keller (North-Holland, Amsterdam, 1980), Vol. 3, p. 1.
- ¹⁰P. A. Fedders and M. W. Muller, J. Phys. Chem. Solids **45**, 685 (1984).
- ¹¹A. B. Chen and A. Sher, Phys. Rev. B **32**, 3695 (1985).
- ¹²J. L. Martins and A. Zunger, Phys. Rev. B **30**, 6217 (1984).
- ¹³G. P. Srivastava, J. L. Martins, and A. Zunger, Phys. Rev. B **31**, 2561 (1985). See Phys. Rev. B **38**, 12 694(E) (1988).
- ¹⁴A. A. Mbaye, L. G. Ferreira, and A. Zunger, Phys. Rev. Lett. **58**, 49 (1987); L. G. Ferreira, A. A. Mbaye, and A. Zunger, Phys. Rev. B **37**, 10 547 (1988).
- ¹⁵J. L. Martins and A. Zunger, J. Mater. Res. **1**, 523 (1986).
- ¹⁶K. Msumoto, S. Isomura, and K. Sasaki, Phys. Status Solidi A **6**, 515 (1971).
- ¹⁷S.-H. Wei and A. Zunger, Phys. Rev. Lett. **56**, 2391 (1986); Phys. Rev. B **35**, 2340 (1987).
- ¹⁸J. L. Martins and A. Zunger, Phys. Rev. Lett. **56**, 1400 (1986).
- ¹⁹A. A. Mbaye, D. M. Wood, and A. Zunger, Phys. Rev. B **37**, 3008 (1988); Appl. Phys. Lett. **49**, 782 (1986).
- ²⁰C. P. Flynn, Phys. Rev. Lett. **57**, 599 (1986).
- ²¹D. M. Wood, S.-H. Wei, and A. Zunger, Phys. Rev. B **37**, 1342 (1988); Phys. Rev. Lett. **58**, 1123 (1987).
- ²²J. E. Bernard and A. Zunger, Phys. Rev. B **34**, 5992 (1986); **36**, 3199 (1987).
- ²³J. E. Bernard, S.-H. Wei, D. M. Wood, and A. Zunger, Appl. Phys. Lett. **52**, 311 (1988).
- ²⁴A. Zunger and J. E. Jaffe, Phys. Rev. Lett. **51**, 662 (1983).
- ²⁵S.-H. Wei and A. Zunger, J. Appl. Phys. **63**, 5794 (1988).
- ²⁶S. Krishnamurthy, M. A. Berding, A. Sher, and A.-B. Chen, Phys. Rev. B **37**, 4254 (1988); A.-B. Chen and A. Sher, Phys. Rev. Lett. **40**, 900 (1978).
- ²⁷R. J. Lempert, K. C. Hass, and H. Ehrenreich, Phys. Rev. B **36**, 1111 (1987); K. C. Hass, H. Ehrenreich, and B. Velicky, *ibid.* **27**, 1088 (1983).
- ²⁸T. Fukui and H. Saito, Jpn. J. Appl. Phys. **23**, L521 (1984).
- ²⁹T. S. Kuan, W. I. Wang, and E. L. Wilkie, Appl. Phys. Lett. **51**, 51 (1987).
- ³⁰T. S. Kuan, T. F. Kuech, W. I. Wang, and E. L. Wilkie, Phys. Rev. Lett. **54**, 201 (1985).
- ³¹H. R. Jen, M. J. Cherng, and G. B. Stringfellow, Appl. Phys. Lett. **48**, 1603 (1986); H. R. Jen, M. J. Cheng, M. J. Jou, and G. B. Stringfellow, in *GaAs and Related Compounds 1986*, Inst. Phys. Conf. Ser. No. 83, edited by W. T. Lindley (IOP, London, 1987), p. 159.
- ³²I. J. Murgatroyd, A. G. Norman, and G. R. Booker (unpublished); Y. E. Ihm, N. Otuska, J. Klem, and H. Morkoç, Appl. Phys. Lett. **51**, 2013 (1987); J. Klem, D. Huang, H. Morkoç, Y. E. Ihm, and N. Otsuka, *ibid.* **50**, 1364 (1987); D. Huang, J. Chyi, J. Klem, and H. Morkoç, J. Appl. Phys. **58**, 5859 (1988).
- ³³(a) A. Gomyo, T. Suzuki, and S. Iijima, Phys. Rev. Lett. **60**, 2645 (1988); A. Gomyo, T. Suzuki, K. Kobayashi, S. Kawatu, and I. Hino, Appl. Phys. Lett. **50**, 673 (1987); A. Gomyo, K. Kobayashi, S. Kawata, I. Hino, and T. Suzuki, J. Cryst. Growth **77**, 367 (1986); (b) S. R. Kurtz, J. M. Olson, and A. Kibbler, Solar Cells **24**, 307 (1988); (c) P. Bellon, J. P. Chevalier, G. P. Martin, E. Dupont-Nivet, C. Thiebaut, and J. P. André, Appl. Phys. Lett. **52**, 567 (1988); M. Kondow, H. Kakibayashi, and S. Minagawa, J. Cryst. Growth **88**, 291 (1988); S. McKernan, B. C. DeCooman, C. B. Carter, D. P. Bour, and J. R. Shealy, J. Mater. Res. **3**, 406 (1988); O. Ueda, M. Takikawa, J. Komeno, and I. Umebu, Jpn. J. Appl. Phys. **26**, L1824 (1987).
- ³⁴A. G. Norman, R. E. Mallard, I. J. Murgatroyd, G. R. Booker, A. H. Moore, and M. D. Scott, in *Microscopy of Semiconductor Materials*, Inst. Phys. Conf. Ser. No. 87, edited by A. G. Cullis and P. D. Augustus (IOP, London, 1987), p. 77.
- ³⁵M. A. Shahid, S. Mahajan, D. E. Laughlin, and H. M. Cox, Phys. Rev. Lett. **58**, 2567 (1987).
- ³⁶H. Nakayama and H. Fujita, in *Gallium Arsenide and Related Compounds 1985*, Inst. Phys. Conf. Ser. No. 79, edited by M. Fujimoto (Hilger, Boston, 1986), p. 289; Y. Matsui, H. Hayashi, and K. Hoshida, Appl. Phys. Lett. **48**, 1060 (1986).
- ³⁷L. G. Ferreira, S.-H. Wei, and A. Zunger (unpublished); D. M. Wood and A. Zunger, Phys. Rev. Lett. **61**, 1501 (1988).
- ³⁸M. Garriga, M. Cardona, N. E. Christensen, P. Lautenschlager, T. Isu, and K. Ploog, Phys. Rev. B **36**, 3254 (1987).

- ³⁹M. Cardona, T. Suemoto, N. E. Christensen, T. Isu, and K. Ploog, *Phys. Rev. B* **36**, 5906 (1987).
- ⁴⁰L. D. Landau and E. M. Lifshitz, *Statistical Physics* (Pergamon, Oxford, 1969), Chap. 14.
- ⁴¹D. de Fontain, in *Solid State Physics*, edited by H. Ehrenreich, F. Seitz, and D. Turnbull (Academic, New York, 1979), Vol. 37, p. 73.
- ⁴²*International Tables for Crystallography*, edited by T. Hahn (Reidel, Dordrecht, 1983), Vol. A.
- ⁴³P. Villars and L. D. Calvert, *Pearson's Handbook of Crystallographic Data for Intermetallic Phases* (American Society for Metals, Metals Park, OH, 1985), Vols. 1–3.
- ⁴⁴E. Parthé, *Crystal Chemistry of Tetrahedral Structures* (Gordon and Breach, New York, 1964).
- ⁴⁵A. G. Khachaturyan, *Theory of Structural Transformations in Solids* (Wiley, New York, 1983).
- ⁴⁶*Landolt-Börnstein: Numerical Data and Functional Relationships in Science and Technology*, edited by P. Eckerlin and H. Kandler (Springer-Verlag, Berlin, 1971), Vol. III/6.
- ⁴⁷*Binary Alloy Phase Diagrams*, edited by J. L. Murray, L. H. Bennett, and H. Baker (American Society for Metals, Metals Park, OH, 1986), Vols. 1–3.
- ⁴⁸M. Lax, *Symmetry Principles in Solid State and Molecular Physics* (Wiley, New York, 1974), p. 443.
- ⁴⁹J. E. Bernard, L. G. Ferreira, S.-H. Wei, and A. Zunger, *Phys. Rev. B* **38**, 6338 (1988).
- ⁵⁰S. S. Vishnubhatla, B. Eyglunent, and J. C. Woolley, *Can. J. Phys.* **47**, 1661 (1986).
- ⁵¹O. Berolo, J. C. Wooley, and J. A. VanVechten, *Phys. Rev. B* **8**, 3794 (1973); O. Berolo and J. C. Wooley, *Can. J. Phys.* **49**, 1335 (1971).
- ⁵²J. A. Vechten and T. K. Bergstresser, *Phys. Rev. B* **1**, 3351 (1970).
- ⁵³A. Baldereschi, E. Hess, K. Maschke, H. Neumann, K. R. Schulze, and K. Unger, *J. Phys. C* **10**, 4709 (1977).
- ⁵⁴R. Hill and D. Richardson, *J. Phys. C* **4**, L289 (1971); **4**, L339 (1971).
- ⁵⁵K. E. Neuman and J. D. Dow, *Phys. Rev. B* **27**, 7495 (1983).
- ⁵⁶A.-B. Chen and A. Sher, *Phys. Rev. Lett.* **40**, 900 (1978); *Phys. Rev. B* **23**, 5360 (1981); **22**, 3886 (1980).
- ⁵⁷R. Hill, *J. Phys. C* **7**, 521 (1974).
- ⁵⁸H. Krakauer (unpublished); S.-H. Wei, Ph.D. thesis, College of William and Mary, 1985, p. 110 (unpublished).
- ⁵⁹W. A. Harrison, *Electronic Structure and the Properties of Solids* (Freeman, San Francisco, 1980).
- ⁶⁰A. G. Thompson, M. Cardona, K. L. Shaklee, and J. C. Woolley, *Phys. Rev.* **146**, 601 (1966).
- ⁶¹D. Stroud, *Phys. Rev. B* **5**, 3366 (1972).
- ⁶²S.-H. Wei and H. Krakauer, *Phys. Rev. Lett.* **55**, 1200 (1985); S.-H. Wei, H. Krakauer, and M. Weinert, *Phys. Rev. B* **32**, 7792 (1985), and references therein.
- ⁶³P. Hohenberg and W. Kohn, *Phys. Rev.* **136**, B864 (1964); W. Kohn and L. J. Sham, *ibid.* **140**, A1133 (1965).
- ⁶⁴(a) J. P. Perdew and A. Zunger, *Phys. Rev. B* **23**, 5048 (1981); (b) D. M. Ceperley and B. J. Alder, *Phys. Rev. Lett.* **45**, 566 (1980).
- ⁶⁵L. Hedin and B. I. Lundquist, *J. Phys. C* **4**, 1064 (1971).
- ⁶⁶A. H. MacDonald, W. E. Pickett, and D. D. Koelling, *J. Phys. C* **13**, 2675 (1980); W. E. Pickett, J. A. Freeman, and D. D. Koelling, *Phys. Rev. B* **23**, 1266 (1981).
- ⁶⁷D. J. Chadi and M. L. Cohen, *Phys. Rev. B* **8**, 5747 (1973); H. J. Monkhorst and J. D. Pack, *ibid.* **13**, 5188 (1976).
- ⁶⁸D. Singh, H. Krakauer, and C. S. Wang, *Phys. Rev. B* **34**, 8391 (1986); C. G. Broyden, *Math. Comput.* **19**, 577 (1965).
- ⁶⁹*Landolt-Börnstein: Numerical Data and Functional Relationships in Science and Technology*, edited by O. Madelung, M. Schulz, and H. Weiss (Springer-Verlag, Berlin, 1982), Vol. 17a. See also data collected in Ref. 21 for the structural properties. For the deformation potential, see also data collected in Ref. 72 below. For spin-orbit splitting, see also T.-C. Chang and D. E. Eastman, *Phys. Rev. B* **22**, 2940 (1980), and Ref. 83 below.
- ⁷⁰The cohesive energy is obtained by subtracting from the measured formation enthalpies from the compilation by O. Kubaschewski and C. B. Alcock [*Metallurgical Thermochemistry*, 5th ed. (Pergamon, Oxford, 1979), pp. 268–286] the cohesive energies of elemental solids quoted by C. Kittel, in *Introduction to Solid State Physics*, 6th ed. (Wiley, New York, 1986).
- ⁷¹A. Fazzio, M. J. Caldas, and A. Zunger, *Phys. Rev. B* **30**, 3430 (1984). See also Ref. 64.
- ⁷²N. E. Christensen, *Phys. Rev. B* **30**, 5753 (1984).
- ⁷³K. J. Chang, S. Froyen, and M. L. Cohen, *Solid State Commun.* **50**, 105 (1984).
- ⁷⁴J. R. Chelikowsky and M. L. Cohen, *Phys. Rev. B* **14**, 556 (1976).
- ⁷⁵M. L. Cohen and T. K. Bergstresser, *Phys. Rev.* **141**, 789 (1966).
- ⁷⁶P. Vogl, H. P. Hjalmarson, and J. P. Dow, *J. Phys. Chem. Solids* **44**, 365 (1983).
- ⁷⁷T. N. Morgan, *Phys. Rev. Lett.* **21**, 819 (1968).
- ⁷⁸(a) D. M. Wood, A. Zunger, and R. de Groot, *Phys. Rev. B* **31**, 2570 (1985); A. E. Carlsson, A. Zunger, and D. M. Wood, *ibid.* **32**, 1386 (1985); S.-H. Wei and A. Zunger, *Phys. Rev. Lett.* **56**, 528 (1986); (b) S. L. Richardson and M. L. Cohen, *Phys. Rev. B* **35**, 1388 (1987), have also observed that $X_{3c}(\text{GaSb})$ is below $X_{1c}(\text{GaSb})$.
- ⁷⁹S.-H. Wei and A. Zunger (unpublished); S. Froyen, S.-H. Wei, and A. Zunger, *Phys. Rev. B* **38**, 10 124 (1988).
- ⁸⁰D. J. Chadi and M. L. Cohen, *Phys. Status Solidi B* **68**, 405 (1975).
- ⁸¹A. D. Prins, J. D. Cambkin, D. J. Dunstan, and I. G. Spain (unpublished).
- ⁸²See data collected in R. W. Godby, M. Schlüter, and L. J. Sham, *Phys. Rev. B* **35**, 4170 (1987), and in Ref. 69. For the valence states, see also G. P. Williams, F. Cerrina, G. J. Lapre, J. R. Anderson, R. J. Smith, and J. Hermanson, *Phys. Rev. B* **34**, 5548 (1986). The experimental results for the higher X_c state are not very certain. Uncertainty in the experiment data for conduction states are ~ 0.1 and ~ 0.2 eV for valence states. We have added $\frac{1}{3}$ of the spin-orbit splitting Δ_0 to the experimental data whenever it is applicable.
- ⁸³L. Lay, R. A. Pollak, F. R. McFeely, S. R. Kowalczyk, and D. A. Shirley, *Phys. Rev. B* **19**, 600 (1974); P. J. Ireland, L. L. Kazmerski, and R. F. Fisher, *J. Vac. Sci. Technol. A* **2**, 1129 (1984).
- ⁸⁴A. Zunger, *Phys. Rev. Lett.* **50**, 1215 (1983).
- ⁸⁵L. Vegard, *Z. Phys.* **5**, 17 (1921).
- ⁸⁶J. C. Mikkelsen and J. B. Boyce, *Phys. Rev. Lett.* **49**, 1412 (1982); *Phys. Rev. B* **28**, 7130 (1983).
- ⁸⁷S.-H. Wei and A. Zunger, *Phys. Rev. Lett.* **59**, 144 (1987); *J. Vac. Sci. Technol. B* **5**, 1239 (1987).
- ⁸⁸S. P. Kowalczyk, J. T. Cheung, E. A. Kraut, and R. W. Grant, *Phys. Rev. Lett.* **56**, 1605 (1986).
- ⁸⁹S.-H. Wei and A. Zunger, *J. Vac. Sci. Technol. A* **6**, 2597 (1988), and experimental references quoted therein.
- ⁹⁰We use the term values given in Table IV and the coupling parameters of Harrison [W. A. Harrison, *Phys. Rev. B* **24**, 5835

- (1981)]. See Ref. 87 for details.
- ⁹¹Data are taken from M. Jaros, Phys. Rev. B **37**, 7112 (1988).
- ⁹²A. D. Katnani and G. Margaritondo, Phys. Rev. B **28**, 1944 (1983).
- ⁹³In Fig. 5, the Γ_{1c} state of GaAs is about 0.06 eV higher than that of GaSb on an absolute energy scale. However, in ternary compounds GaAs is expanded and GaSb is compressed. Since the deformation potential of the Γ_{1c} state is positive, lattice deformation lowers the energy of Γ_{1c} (GaAs) below that of Γ_{1c} (GaSb). We find that a better indication of relative ordering of the states is given by the atomic energies of the orbitals associated with the states.
- ⁹⁴In the CuPt Brillouin zone, the point $(\frac{1}{2}, \frac{1}{2}, 0)$ (and cyclic permutations), expressed in terms of the reciprocal translation vector $b_1 = (\pi/a)(3\hat{x} - \hat{y} - \hat{z})$ (and cyclic permutations) are folded from X and L points of the zinc-blende Brillouin zone.
- ⁹⁵E. Yamaguchi, Extended Abstracts of the 19th Conference on Solid State Devices and Materials, Tokyo, 1987, p. 483 (unpublished). See also S. H. Wei and A. Zunger, Appl. Phys. Lett. **53**, 2077 (1988).
- ⁹⁶(a) The Pauling electronegativities are compiled in *Table of Periodic Properties of the Elements* (Sargent-Welch Scientific Co., Skokie, IL, 1980); (b) L. Pauling, *The Nature of the Chemical Bond* (Cornell University Press, Ithaca, NY, 1960), p. 246.
- ⁹⁷H. J. Lee, L. Y. Juravel, J. C. Woolley, and A. J. SpringThorpe, Phys. Rev. B **21**, 659 (1980); H. C. Casey, Jr., Appl. Phys. **49**, 3684 (1978); M. A. Afronowitz, Solid State Commun. **15**, 59 (1974).
- ⁹⁸T. Isu, D. S. Jiang, and K. Ploog, Appl. Phys. **43**, 75 (1987).
- ⁹⁹A. Ishibashi, Y. Mori, M. Itabashi, and N. Watanabe, J. Appl. Phys. **58**, 2691 (1985).
- ¹⁰⁰M. D. Sturge, E. Cohen, and R. A. Logan, Phys. Rev. B **27**, 2362 (1983); M. V. Klein, M. D. Sturge, and E. Cohen, *ibid.* **25**, 4331 (1982).
- ¹⁰¹T. Nishino, Y. Inoue, Y. Hamakawa, M. Kondo, and S. Minagawa, Appl. Phys. Lett. **53**, 583 (1988).
- ¹⁰²In ternary ordered compounds, the fourfold-degenerate zinc-blende Γ_8 state is further split into two twofold states due to the crystal field (except luzonite structure). To determine $\Delta_0(X_n)$, we have taken the average of the two crystal-field-split states. Since $\Delta_0 \gg \Delta_{CF}$, this procedure is expected to introduce only small errors (~ 0.02 eV for CuPt structure and much less for the others). See J. L. Shay and J. H. Wernick, *Ternary Chalcopyrite Semiconductors: Growth, Electronic Properties, and Applications* (Pergamon, Oxford, 1975), p. 82.
- ¹⁰³R. Hill, J. Phys. C **7**, 521 (1974).
- ¹⁰⁴W. Porod and D. K. Ferry, Phys. Rev. B **27**, 2587 (1983).
- ¹⁰⁵A. A. El-Shazly, M. M. H. El-Naby, M. A. Kenawy, M. M. El-Nahass, H. T. El-Shair, and A. M. Ebrahim, Appl. Phys. A **36**, 51 (1985); R. Mach, P. Flgel, L. G. Suslina, A. G. Areshkin, J. Maege, and G. Voigt, Phys. Status Solidi B **109**, 607 (1982).
- ¹⁰⁶A. Ebina, M. Yamamoto, and T. Takahashi, Phys. Rev. B **6**, 3786 (1972).
- ¹⁰⁷S. Larach, R. E. Shrader, and C. F. Stocker, Phys. Rev. **108**, 587 (1957); R. Hill and D. Richardson, J. Phys. C **6**, L115 (1973).
- ¹⁰⁸M. B. Thomas, W. M. Coderre, and J. C. Woolley, Phys. Status Solidi A **2**, K141 (1970); R. E. Nahory, M. A. Pollack, J. C. DeWinter, and K. M. Williams, J. Appl. Phys. **48**, 1607 (1977); G. A. Antypas and L. W. James, *ibid.* **41**, 2165 (1970); R. M. Cohen, M. J. Cherng, R. E. Benner, and G. B. Stringfellow, *ibid.* **57**, 4817 (1985).
- ¹⁰⁹H. J. Lee, L. Y. Juravel, and J. C. Woolley, Phys. Rev. B **21**, 659 (1980); C. Bosio, J. L. Staehli, M. Guzzi, G. Burri, and R. A. Logan, *ibid.* **38**, 3263 (1988). See compilation of experimental data in its Table II.
- ¹¹⁰R. Dingle, R. A. Logan, and J. R. Arthur, Jr., in *Gallium Arsenide and Related Compounds*, Inst. Phys. Conf. Ser. No. 33a, edited by C. Hilsum (IOP, Bristol, 1977), p. 210; H. C. Casey, Jr., J. Appl. Phys. **49**, 3684 (1978).
- ¹¹¹M. Posternak, A. Baldereschi, S. Massidda, and A. J. Freeman, in Proceedings of the 14th International Symposium on GaAs and Related Compounds (Heraklion, Crete, Greece, 1987) (unpublished).
- ¹¹²B. Monemar, K. K. Shih, and G. D. Pettit, J. Appl. Phys. **47**, 2604 (1976); B. Monemar, Phys. Rev. B **8**, 5711 (1973).
- ¹¹³P. M. Laufer, R. H. Pollak, R. E. Nahory, and M. A. Pollack, Solid State Commun. **36**, 419 (1980).
- ¹¹⁴E. H. Perea, E. E. Mendez, and C. C. Fonstad, Appl. Phys. Lett. **36**, 978 (1980).
- ¹¹⁵Y. Yamazoe, Ph.D. thesis, Osaka University, 1981 (unpublished).
- ¹¹⁶P. Parayanthal and F. H. Pollak, Phys. Rev. B **28**, 3632 (1983).
- ¹¹⁷S. M. Kelso, D. E. Aspnes, M. A. Pollack, and R. E. Nahory, Phys. Rev. B **26**, 6669 (1982).
- ¹¹⁸P. Parayanthal, C. S. Ro, F. H. Pollak, S. R. Stanley, G. W. Wicks, and L. F. Eastman, Appl. Phys. Lett. **43**, 109 (1983).
- ¹¹⁹O. Berolo and J. C. Woolley, in *Proceedings of the Eleventh International Conference on the Physics of Semiconductors*, edited by M. Miasek (PWN/Polish Scientific, Warsaw, 1972), p. 1420.
- ¹²⁰J. A. Van Vechten, O. Berolo, and J. C. Woolley, Phys. Rev. Lett. **29**, 1400 (1972).
- ¹²¹H. Lange, J. Donecker, and H. Friedrich, Phys. Status Solidi B **73**, 633 (1976).
- ¹²²K. J. Bachmann, F. A. Thiel, and H. Schreiber, Prog. Cryst. Growth Charact. **2**, 171 (1979).
- ¹²³A. G. Thompson and J. C. Woolley, Can. J. Phys. **45**, 255 (1967).
- ¹²⁴A. Ebina, M. Yamamoto, and T. Takahashi, Phys. Rev. B **6**, 3786 (1972); A. Ebina, Y. Sato, and T. Takahashi, Phys. Rev. Lett. **32**, 1366 (1974).
- ¹²⁵R. Hill, J. Phys. C **7**, 516 (1974).
- ¹²⁶D. J. Chadi, Phys. Rev. B **16**, 790 (1977).
- ¹²⁷M. F. Ling and D. J. Miller, Phys. Rev. B **34**, 7388 (1986).